A FIBER OPTIC PRESSURE TRANSDUCER

Gordon William Margerum

NAVAL POSTGRADUATE SCHOOL
Monterey, California

THESIS

A FIBER OPTIC PRESSURE TRANSDUCER

by

Gordon William Margerum

Thesis Advisor: A. E. Fuhs

June 1972

A Fiber Optic Pressure Transducer

by

Gordon William Margerum
Lieutenant Commander, United States Navy
B.S., Carnegie Institute of Technology, 1957

Submitted in partial fulfillment of the
requirements for the degree of

AERONAUTICAL ENGINEER

from the

NAVAL POSTGRADUATE SCHOOL
June 1972

ABSTRACT

A pressure transducer with an outside diameter of 0.190" has been built and statically tested. The transducer used a glass fiber bundle 0.109" in diameter to transmit and receive reflected light from a pressure diaphragm. The amount of light returned to a photosensor was dependent upon the diaphragm shape and relative position from the optic fiber bundle. The response was linear over a pressure range which was dependent upon the diaphragm thickness. Several fiber optic probes with different fiber distributions were tested. The random fiber distribution gave the greatest sensitivity. However, with suitable choice of gain selection, pressure range could be sacrificed for increased pressure resolution for any combination of fiber distribution and diaphragm thickness.

A theory was developed for a coaxial fiber distribution with the source light transmitted by the inner circle of fibers and operating with reflection from a flat surface. The theory provided a response curve shape which compared with the measured response.

TABLE OF CONTENTS

LIST OF ILLUSTRATIONS

TABLE OF SYMBOLS AND ABBREVIATIONS

a	individual fiber radius (inches)
d	distance between probe end and undeflected diaphragm (inches)
D	diaphragm diameter (inches)
E	elastic modulus of diaphragm material (pounds per square inch)
f_{01}	first fundamental resonant frequency of diaphragm (Hertz)
F	luminous flux (lumens)
I	illumination (lumens per square foot)
L	fiber length (inches)
n	refraction index; subscripts 0, 1 and 2 refer to the incident, fiber core and cladding media, respectively
NA	numerical aperture
p	diaphragm pressure (pounds per square inch)
r	radius (inches)
R	ratio of outer to inner fiber bundle radius for the coaxial probe
$\mathbb{R}$	Fresnel reflection loss
t	diaphragm thickness (inches)
T	fiber and face transmission factor
u	a parameter defined as $(2d/r_1)\tan\theta$
x	diaphragm deflection (inches)
x_0	diaphragm center deflection (inches)
α	internal reflectivity
β	absorption coefficient
Δ	incremental change in parameter following symbol

θ	angle of light ray in fiber core material (subscript c for critical ray angle; primed angles pertain to incident light; units in degrees)
ν	Poisson's ratio
ρ	diaphragm material density (pounds per cubic inch)
τ	relative transmission
ϕ	slope of pressurized diaphragm (radians)
CTI	coaxial transmitting inside fiber distribution
CTO	coaxial transmitting outside fiber distribution
R	random fiber distribution
kHz	kilohertz
mil	0.001 inches

ACKNOWLEDGEMENT

The author wishes to express his deepest gratitude to Professor Allen E. Fuhs for his assistance, guidance and time and to Naval Postgraduate School technician Mr. Bertis H. Funk for his invaluable technical services.

I. INTRODUCTION

There are numerous test situations where extremely small transducers are essential. Testing of axial flow compressors represents one such application. For determining the influence of distorted inlet flow many, up to 100, transducers are needed.

Presently for this application two types of pressure transducer are used. One type is the semi-conductor strain gage with the strain gages deposited directly on the diaphragm. The other type is the piezoelectric transducer. Both of these transducers have serious deficiencies. Temperature sensitivity of the calibration makes it necessary to conduct in-situ calibration. The strain gage transducers are both costly and fragile. Small particles of dirt in the air stream can, and frequently do, destroy the transducer diaphragm.

A new type of transducer is considered here. The initial concept was to use two optical glass fibers, one of which transmits light to the pressure diaphragm. Reflected light from the diaphragm inner surface is collected and transmitted by an output fiber to a light sensitive element. The output flux, being a function of the diaphragm shape and relative distance from the fiber ends, becomes a measure of diaphragm pressure.

This transducer may be made extremely small – the size of the lead in a pencil. The light source and sensor are

remotely located with respect to each other, and the electronics can be remote from the sensor. The optic fiber connection to the pressure sensing head is quite flexible. Such a system should be less expensive than the strain gage or piezoelectric transducer. The fiber optics transducer may be much less temperature sensitive. The goal of this research was to examine the characteristics of the transducer.

Remote illumination and sensing by optical fibers is not new. Applications similar to this include a fiber optic angular displacement transducer [1], a fiber optical pressure transducer for use in ionizing radiation environment [2] or for prosthetics applications [3] and also numerous non-contact proximity detectors [4].

The sections that follow include a discussion of general design considerations, Section II, wherein a uniformly loaded circular diaphragm and basic fiber optics are reviewed along with some discussion of high temperature and frequency response considerations. The transducer design, equipment and test configurations are related in Section III. Section IV covers the response due to the proximity of a fiber optic probe to a flat reflecting surface and included analytical modeling of this arrangement. The experimental transducer performance with several diaphragms and several fiber optic probes is related and discussed in Section V. Conclusions and recommendations for further research are found in Section VI.

II. DESIGN CONSIDERATIONS

A. DIAPHRAGM DESIGN

Using the deflection formula for a thin, circular plate with clamped edges,

$$x_0 = 3(1-\nu^2)D^4p/256Et^3 \qquad (1)$$

theoretical curves were constructed (Figures 1a, b, and c) describing the relation between pressure, maximum diaphragm deflection, thickness and diameter for various materials. Corresponding curves for the fundamental vibrational mode given by the formula [5],

$$f_{01} = 1.8684t\sqrt{E/\rho(1-\nu^2)}\,/\,D^2 \qquad (2)$$

were also developed (Figures 2a, b, and c).

From Figure 1a, it can be seen that for a stainless steel diaphragm of 0.080 inch diameter and a thickness of 2 mils (1 mil = 0.001 inch) the maximum deflection for 100 p.s.i. is approximately 0.2 mils. One would then require an accuracy in measuring deflection of 2 micro-inches for one p.s.i. resolution. The resonant frequency for this diaphragm, from Figure 2a, is seen to be approximately 125 kHz.

Optical proximity detectors are available with a resolution of less than 1 micro-inch and with a corresponding linear range of approximately 4 mils [6].

B. FIBER OPTIC PROBE DESIGN

1. General Fiber Theory [7]

The analysis of light transmission in optical fibers is a waveguide phenomenon. However, for cases where the fiber diameter is much greater than the wavelength of light the methods of geometric optics may be applied. This leads to the principle of total internal reflection which is the basis for fiber optic light transmission.

The fiber generally consists of a cylindrical core material with an index of refraction, n_1, and a cladding material with an index n_2. For total internal reflection from the core-cladding interface to occur, the meridional ray angle measured from the fiber axis, Figure 3a, must be less than a critical angle, θ_c, given by

$$\theta_c = \sin^{-1}[\sqrt{n_1^2 - n_2^2} / n_1] . \qquad (3)$$

In terms of the source ray incident on the core end face, Figure 3b, light is transmitted for incident angles less than

$$\theta_c' = \sin^{-1}[\sqrt{n_1^2 - n_2^2} / n_0] . \qquad (4)$$

This cone of light acceptance, measured in terms of the cone half angle given by θ_c', leads to a method of expressing the light collecting capability of a straight fiber, namely by its "numerical aperture" defined as

$$NA = n_0 \sin \theta_c' \qquad (5)$$

Theoretically with an exit media of the same index as the incident media, a ray leaves the fiber at the same angle that it entered. As a practical matter, however, internal scattering results in exit angles within a cone.

The fibers used in this work were 3 mil flint glass with an index of 1.62 and a cladding glass of index 1.52. The corresponding NA was 0.56 with an acceptance cone half angle of approximately 34°.

Total transmission through a single fiber is reduced by end face Fresnel reflection losses which are a function of the incident angle. For normal incidence this loss is expressed as

$$\mathbb{R} = (n_1-n_0)^2/(n_1+n_0)^2 \qquad (6)$$

The corresponding transmission factor for two end faces is then

$$T^2 = (1-\mathbb{R})^2 \qquad (7)$$

Relative magnitudes will be dependent on the degree of finish. For example, characteristic values of transmission factor, for polished or cut glass fibers are, from Figure 4a, about 0.92 and 0.65 respectively.

An extremely small loss occurs at each internal reflection interface; however, since the number of such reflections is very large for large fiber length-to-diameter ratio, a significant transmission loss may occur. This loss has been expressed by Potter [8] as α^N where N is the number of internal reflections which for meridional rays is

$$N = (L/2a) \tan \theta \qquad (8)$$

A typical value for α is given as 0.9993±0.0001 for glass with a white light source [8]. For a 3 foot long, 3 mil fiber with an NA of 0.56, the number of reflections for maximum incident angle is approximately L/3a or approximately 4,000. Then α^N is 0.061.

A further loss of light is due to attenuation within the optical core material. This loss is dependent upon the ray path length and is expressed as $\exp[-\beta L \sec \theta]$. An average attenuation coefficient, β, for glass is recommended by glass fiber manufacturers to be 0.085 foot^{-1}.

Typical bulk transmission curves are shown in Figures 4a and 4b as functions of total length and wavelength. Both losses increase with increasing angle θ. Consequently, for long fibers, light with rays near $\theta=0$ is transmitted with much less loss. Thus, when meridional rays only are considered and propagation by the cladding is neglected, one is left with an exit beam which is almost collimated. This result is temporarily shelved to be later reviewed in Appendix A and Appendix C.

A more complete analysis of light propagation by a bundle of fibers includes the effects of additional transmission due to skew rays [8], propagation via the cladding [9], bent fibers and/or variable diameter fibers [10], and may include spectral variations in transmission (Figure 4b).

In summary, the intensity distribution for emitted light rays from a single fiber is described by the equation

$$I = I_0 T^2 \alpha^{(L/2a)\tan\theta} e^{-\beta L \sec\theta} \qquad (9)$$

where T, α and β are characteristic of the core glass.

2. Fiber Optic Probe as a Proximity Detector [11]

Consider adjacent transmitting and receiving fibers at the diaphragm end as in Figure 5. When the sending and receiving fibers are in contact with a reflecting flat surface, no light is reflected into the receiving elements. As the distance, d, between the fiber end and the reflecting plane increases, the cone of light, assumed to be of uniform intensity over a cone of half angle equal to that of the incident cone, is permitted to illuminate an increasingly larger area of the reflecting plane. For ideal specular reflection from this surface the amount of light intercepted by the receiving fibers likewise increases. As discussed in the previous section the intensity is not uniform over the cone of light, but for initial understanding it is an adequate approximation.

The relationship between surface displacement, d, and receiver illumination is essentially a linear relation until the entire surface of the receiving fibers is illuminated. At this point the output response curve reaches a maximum. As the displacement increases beyond this point, the illumination of the receiver decreases in approximately inverse proportion to the square of the distance. A typical transmission versus displacement curve is shown in Figure 5. Two

somewhat linear regions exist, one on the near side between points A and B and one on the far side of the curve between points C and D.

3. Fiber Optic Probe Operation with a Pressure Diaphragm

Several factors will have an influence upon the amount of light collected by the probe receiving fibers. These factors are the average displacement between the probe end and the curved diaphragm, the shape of the curved diaphragm and the wall reflections. The effects of the first may be typified by the displacement curve just mentioned. The effects of the last two, when superimposed upon that of the first, will determine the system performance.

If diaphragm curvature and wall reflections were negligible, one would expect that with operation on the near side of Figure 5 the output signal would decrease with increasing pressure. Similarly with operation on the far side the output signal would increase with increasing pressure. Any deviation from this might be attributed to effects of diaphragm shape and wall reflection.

C. HIGH TEMPERATURE APPLICATION

The probes used in this research were, with one exception, glass fiber bundles encased in a PVC sheath and are limited to 300°F. The exception had a 3 inch tip and spiral steel (BX) casing for operation at 600°F. Similar probes have been used with gas cooling jackets and with viewing through a quartz window at external temperatures to 1100°F [12].

Optical fiber bundles are commercially available which have been exposed to 1050°F with no evidence of functional damage [13]. This high temperature performance would indicate that application in an axial flow compressor environment is not unreasonable with regard to temperature.

D. FREQUENCY RESPONSE

The fundamental frequency for a clamped circular plate of various materials and dimensions was given in Figure 2. The higher modes are a factor of 2.09, 3.43, 3.91 and 5.98 above the fundamental [6]. Frequencies in the vicinity of the fundamental and higher modes must be avoided in the transducer design.

The frequency response of the pressure transducer may be limited by the type of photoconductor used. Some photo transistors have a flat frequency response from DC to 30 kHz and to 50 kHz down 3 dB for small signal swings.

III. TRANSDUCER DESIGN AND EQUIPMENT

All pressure transducers had 0.190 inch outside diameter as shown in Figure 6 to accommodate available standard fiber optic probes. The various diaphragms were silver soldered to the tube end, except for three probes with the diaphragm electron beam welded to the tube. A sleeve was provided for the optical probe to insure coaxial orientation of the probe tip.

Several three-foot long glass fiber probes were available having different geometries: random (R), coaxial transmitting outside (CTO), coaxial transmitting inside (CTI) and split (S). These geometries, shown in Figure 6, provided operation over a wide range of linear displacements.

One experimental arrangement is shown in Figure 7. The light source was an incandescent instrument lamp, type GE-253X, which provided a minimum illumination of 750 foot candles over the entire input fiber area. The bulb voltage was 1.5 volt DC. This bulb and DC power supply were found to provide the most stable source intensity of several arrangements tried. Relative transmission was measured by a photomultiplier tube, RCA Model 931A, connected to a laboratory photometer, Pacific Photometric Instrument Model 11. This arrangement was used with both the linear displacement apparatus and the pressure diaphragm as shown.

A second experimental arrangement used a non-contact optical proximity detector, Mechanical Technology Inc.

Fotonic Sensor Model KD-36, as the light source and sensing system. The relative transmission of light from the optic probe was converted by the Fotonic Sensor to a voltage signal of ±1 volt range. This signal output was monitored by a "Digitec" United System Corporation Digital DC Millivoltmeter. The Sensor had multiple sensitivity adjustment, which permitted expansion of the output signal-displacement curve by multiples of two with each discrete gain setting.

All performance measurements were made under static pressure conditions using a Lockheed mobile pressure test panel with capability for pressure measurement to within 0.5 inches of Mercury.

IV. LINEAR DISPLACMENT CURVES AND MODELING

A. DISPLACEMENT CURVES

A curve of relative transmission versus probe-to-surface displacement was obtained for each fiber geometry. Figure 8 shows the displacement curve results for the four geometries.

An ill fated attempt was first made to obtain these curves by using a micrometer with a reflecting face mounted to its moving end. Rotation of the micrometer caused wavy curves due to the variation in reflectivity over the surface; one wavelength corresponded to one revolution of the micrometer. A calibration instrument which provided translation without rotation solved this problem.

A comparison of the displacement curves clearly demonstrates that the displacement for maximum output was dependent upon the fiber geometry. Accordingly, the slopes of the near and far sides of each curve depend upon geometry. In fact, for near side operation considerable flexibility in displacement resolution was available by selection of an appropriate geometry. The near side slope changed by a factor of about 5 for random relative to split fiber geometries. On the other hand, the displacement range dictates the best geometry.

For example, with a random fiber geometry, it was evident from Figure 8 that an approximately linear displacement range of ±3 mils was available from operation in the near region. The initial probe-to-surface displacement required here would

be about 5 mils. Due to the effects of diaphragm curvature and the reflecting tube wall, the displacement curves provide only general guidance in configuration selection. In addition, displacement curves as shown could be expected to differ greatly for a given fiber distribution, CTI for example with a different fiber size and different inner and outer bundle radii.

B. DISPLACEMENT CURVE MODEL

Figure 9 illustrates the geometry for analysis of the coupling for a CTI fiber bundle in conjunction with a flat reflecting surface. The analysis, which is developed in Appendix C, resulted in an equation for the relative transmission which for the near region was of the form

$$\tau = K\, u^2(3+u)/(1+u)^3 \qquad (10)$$

where $u = (2d/r_1)\tan\theta$ and K is a normalizing constant. For the far region the result was of the form

$$\tau = K\,[3u(R^2-1) - (2R^3-3R^2+1)]/(1+u)^3 \qquad (11)$$

where $R = r_2/r_1$.

Recall that these regions are defined in Figure 5. Relative transmission calculated using equations (10) and (11) was compared with the measured CTI displacement curve of Figure 8. The comparison shown in Figure 10 is good for particular values of the parameters. Several values of these parameters, R and θ, were changed to better match the measured curve. However, it was evident that the necessary values of R and θ

for a best match were somewhat different from the actual values for the CTI probe.

It was observed that the point of maximum response was shifted to larger displacement values when the ratio, R, is increased, i.e. with decreasing r_1 and constant r_2. One would intuitively anticipate this result for the CTI probe because a smaller inner bundle would require more displacement to illuminate the entire receiving area.

V. EXPERIMENTAL TRANSDUCER PERFORMANCE AND DISCUSSION

A. PROBE AT NEAR SIDE OF DISPLACEMENT CURVE

A random fiber probe was first tested with a 1 mil. thick steel diaphragm. The pressure available from the apparatus illustrated in Figure 7 was sufficient for deflections approximately five times this thickness. For near side probe position the relative transmission versus pressure response, Figure 11, was linear for very small pressures (less than 10 inches of Hg.). For larger pressures the relative transmission decreases but at a slower rate. This same result was evident in near side operation of the same diaphragm using all other fiber distributions as shown in Figure 11.

From the curves of Figure 1a, which are based upon flat plate theory, it is evident that for this diaphragm a pressure of about 10" Hg corresponds to a centerline deflection nearly equal to the diaphragm thickness. The flat plate theory is based upon the assumption of a neutral middle plane which restricts its application to plate deflections that are small with respect to the plate thickness. Specifically it is seen in Den Hartog [14] that the plate theory is applicable for deflections less than half the thickness. Thus, in Figure 11, only with pressures less than 5 inches of Hg can the response be expected to be described by linear flat plate theory. In equation (1) x_0 varies linearly with p.

Also when a plate is so highly loaded that the center deflection is five times the thickness, non-linear membrane theory applies. For a membrane the center deflection is proportional to the cube root of the pressure. Therefore, for the above case where we remain entirely within the near side linear region of the base curve the response curves of Figure 11 describe diaphragm deflections ranging from linear plate theory through a mixed region to the non-linear membrane theory.

Disregarding the effects due to reflectivity and diaphragm curvature, there is a direct correlation between Figures 8 and 11 within the realm of linear flat plate theory. The initial slope of each curve of Figure 11 is directly proportional to the slope, at about 0.7 relative transmission, of the corresponding curve of Figure 8. The proportionality is given by equation (1), that is x_0/p . A plot of these slopes is shown in Figure 12 which compares this information with a calculated x_0/p from equation (1) for the diaphragm used. The reasonably good comparison is consistent with the calculations of Appendix B which indicate a negligible influence due to diaphragm curvature.

Before discussion of transducer operation with an initial position on the far side of the linear displacement curve, it should be mentioned that at an initial position midway between near and far regions, i.e., at the point of maxima of Figure 8 where there is no response due to displacement,

there was negligible transmission change with pressure. Any change in transmission here could be expected to be due only to diaphragm curvature. The conclusion is that diaphragm curvature has little effect on signal output when operating at the peak of the displacement curve.

B. PROBE AT FAR SIDE OF DISPLACEMENT CURVE

When the initial probe-to-diaphragm displacement was on the far side of the displacement curve, the output signal did not increase with increasing pressure as the displacement curves would suggest. On the contrary, the relative transmission decreased with increasing pressure in a fashion remarkably similar to front side response. Figure 13 shows these results for the coaxial and split geometries. The relative effects of diaphragm curvature are considered to predominate and cause the output signal to decrease with increasing pressure.

C. WALL REFLECTION EFFECTS

No special effort was taken to blacken the inside of the diaphragm tube and thus possibly eliminate extraneous effects of wall reflectivity. An attempt to measure the wall effect was accomplished by comparing pressure-response curves when the fiber optic probe was mounted outside the diaphragm tube with those for normal probe position inside the tube. This data, shown in Figure 14, indicates a difference in pressure-response between the two configurations. It was assumed that the absence of a wall would result in more transmission loss

with increasing diaphragm curvature than when a reflecting wall was present. Thus, without a wall the decrease in relative transmission with increasing pressure would be faster than with a wall. The result would be flatter response curves with an "inside" probe than with a probe outside the cylinder. The data showed just the contrary.

Several factors may contribute individually or in combination to yield such results. Due to non-uniformities in the silver soldered diaphragm-to-tube joint, the shape of the diaphragm when deflected in one direction may not correspond to the shape when pressurized from the opposite side. If the diaphragm were not truly flat in the unloaded condition, the shape assumed when pressurized from different sides would not necessarily be the same. Also the distance between the unloaded diaphragm and the fiber probe tip for inside and outside operation was not accurately measured.

D. PERFORMANCE WITH HIGHER RESOLUTION

The light intensity at the photomultiplier during pressure application to the diaphragm was little different from that at zero pressure. The necessary bias for zero pressure intensity resulted in a laboratory photometer/photomultiplier combination which had insufficient sensitivity to yield response curves adequate for good resolution of pressure. The Fotonic Sensor, Model KD-36, was used as mentioned in Section III in order to provide better resolution. This unit had a second photocell for monitoring the source light intensity for differential measurements.

A plot of signal output vs. pressure is shown in Figure 15 for a probe with random fiber distribution operating near the 1 mil thick steel diaphragm. This linear output at low pressures was similar to previous results. This curve was obtained at the lowest instrument gain.

Similar results were obtained with a CTI probe and the same diaphragm. The same non-linear output resulted, Figure 16, when the diaphragm was overloaded. Also a slight hysteresis is noticeable here. This was believed to be the result of the working of the soldered diaphragm-to-tube joint which would experience local failure after numerous high pressure cycles. A large hysteresis was noticeable when pressure cycles went to a level where the diaphragm stress was close to the material yield stress.

Figure 17 shows the output signal vs. pressure plot for a CTO probe at several gain settings of the Fotonic Sensor. At the higher gain a better resolution of pressure is available with some sacrifice in pressure range.

An increasing diaphragm thickness greatly increases the maximum pressure corresponding to a deflection equal to half the plate thickness. From equation (1) the maximum pressure is proportional to the fourth power of thickness. Thus with a thicker plate, a larger pressure range is handled at lower sensor gains with fairly good resolution. Figure 18 shows an output signal pressure plot for near side operation of a probe with random fiber distribution. The diaphragm was 0.003" thick brass. The response was quite linear up to 60 inches of Mercury.

VI. CONCLUSIONS AND RECOMMENDATIONS

A fiber optic pressure transducer has been developed with a linear response. Parameters of design, such as diaphragm diameter and thickness, optic fiber bundle geometry and probe-to-diaphragm initial displacement, have varying effects upon the system performance.

The modeling of the linear displacement curve provided a reasonable first approximation to the measured results. Further development is necessary to describe and specify diaphragm response and related signal outputs.

Some consideration should be given to development of a smaller probe with different diaphragm mounting. A smaller size is believed better suited to the multiple location pressure monitoring requirements of axial flow compressor research.

Dynamic pressure tests are necessary using a photo cell with a short rise time. The transducer should be tested to insure that the amplitude response is not frequency dependent. A fiber optic proximity detector responsive to at least 50 kHz should be considered.

Temperature sensitivity tests of the transducer are needed to more clearly identify the temperature effects upon the diaphragm.

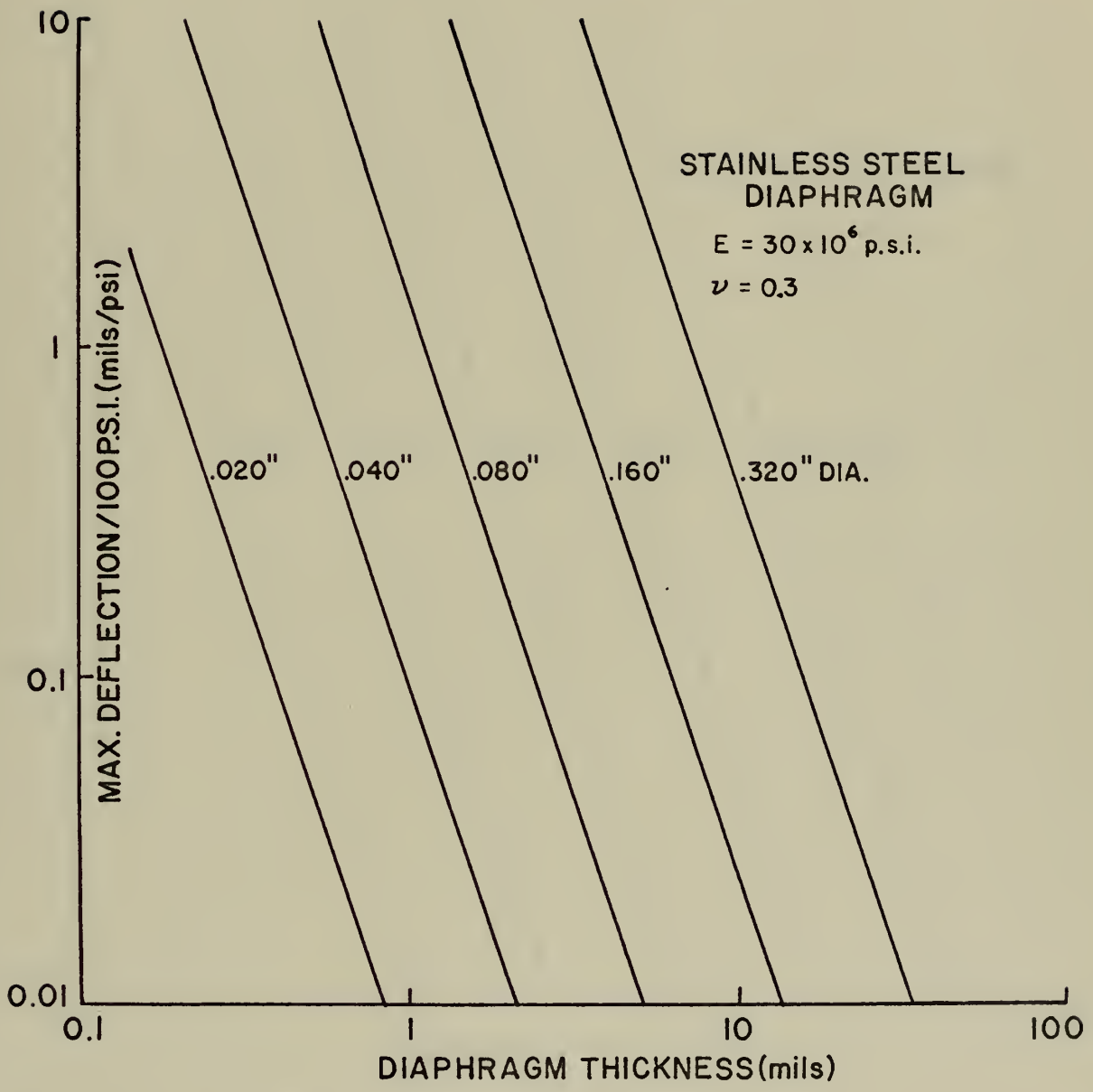

Figure 1a. Diaphragm Maximum Deflection, Stainless Steel

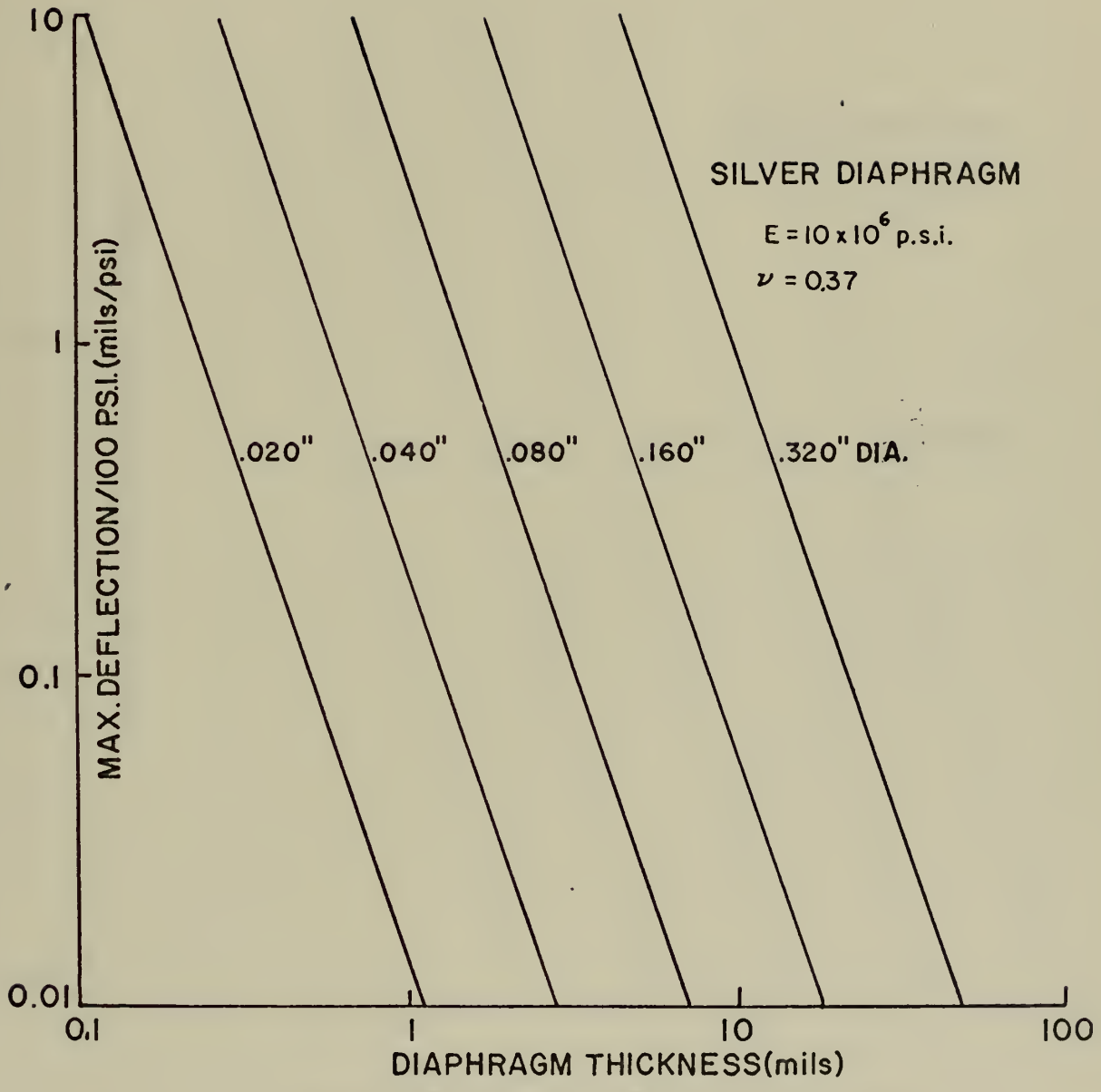

Figure 1b. Diaphragm Maximum Deflection, Silver

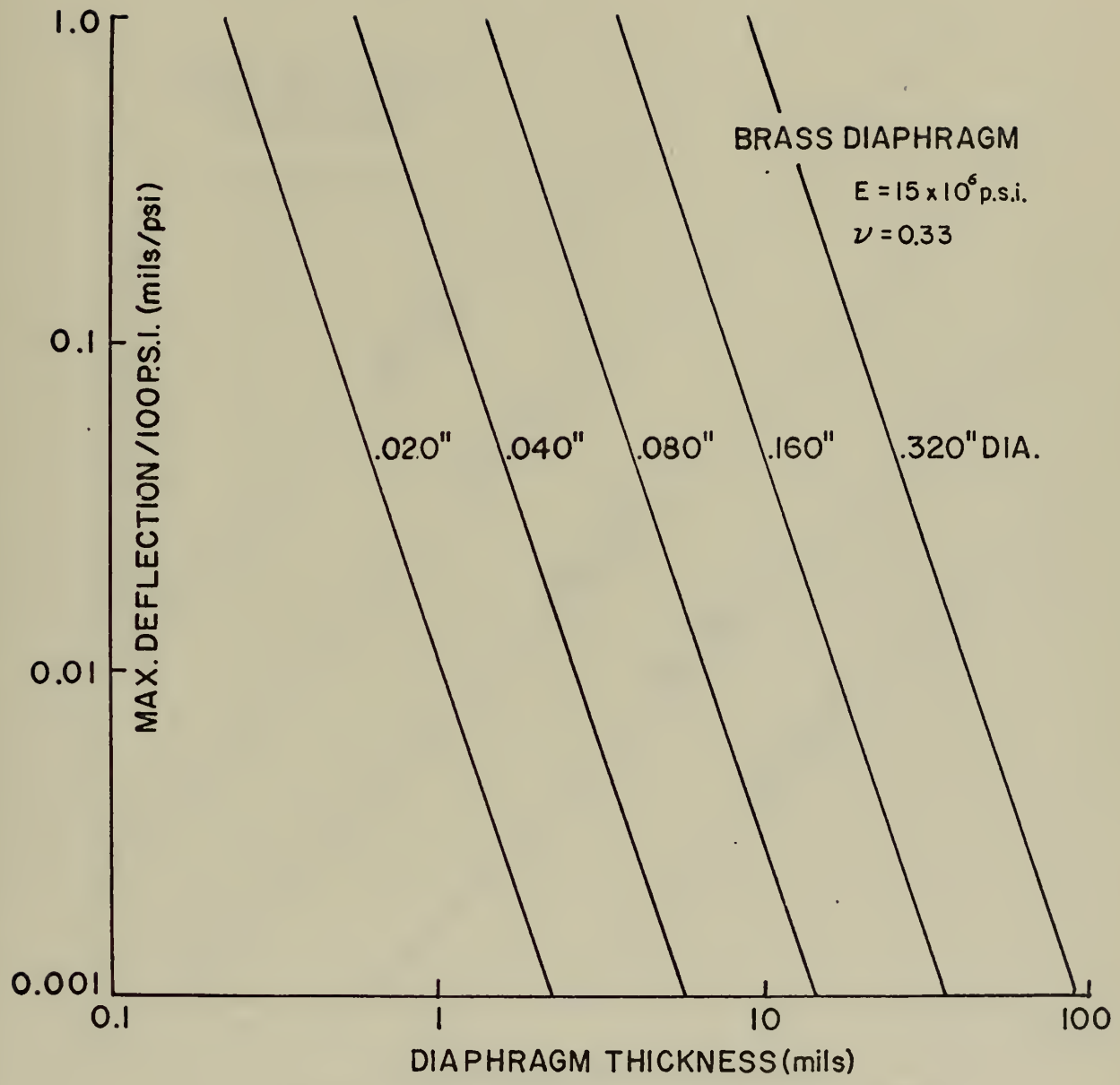

Figure 1c. Diaphragm Maximum Deflection, Brass

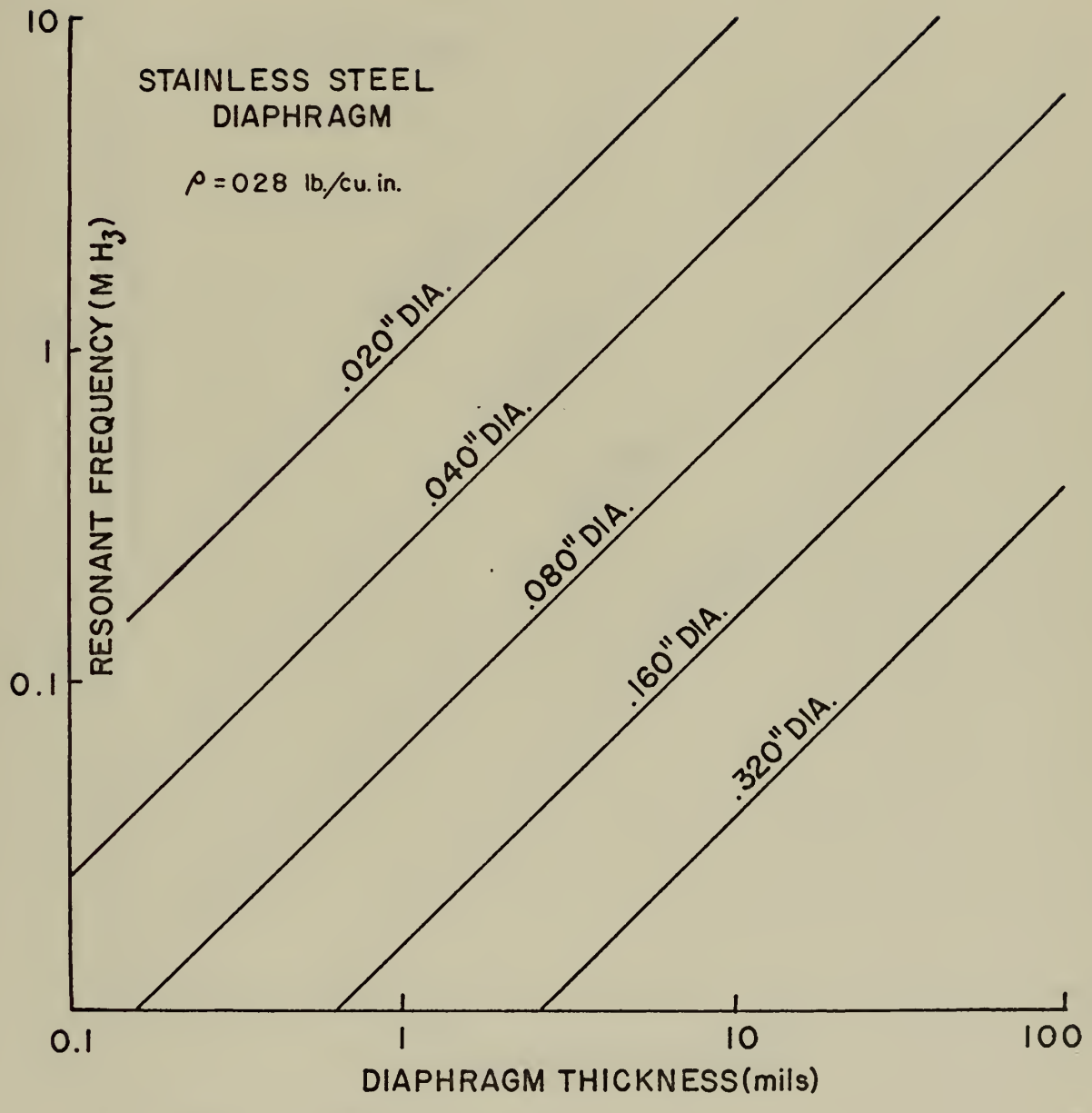

Figure 2a. Diaphragm Fundamental Resonant Frequency, Stainless Steel

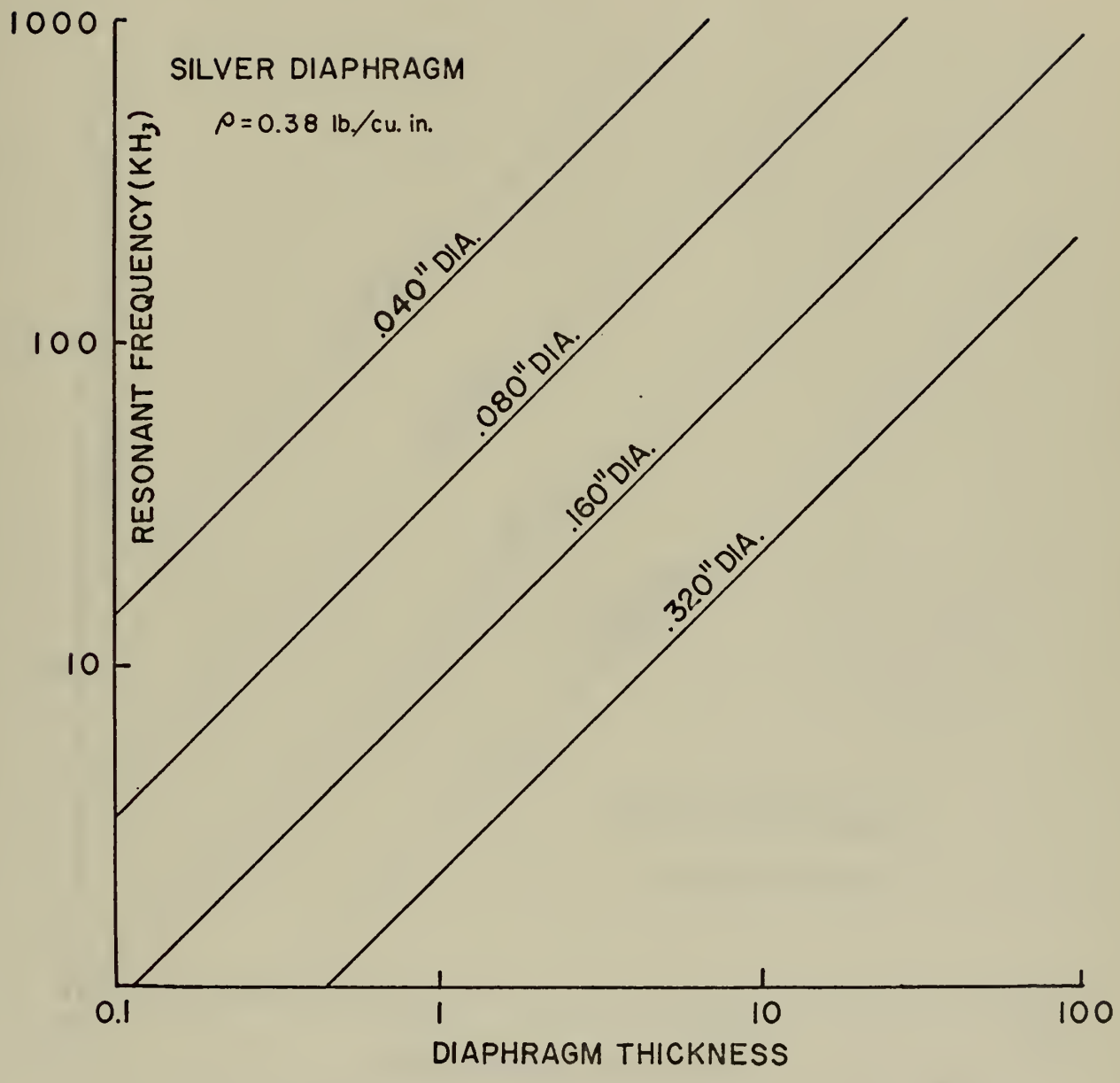

Figure 2b. Diaphragm Fundamental Resonant Frequency, Silver

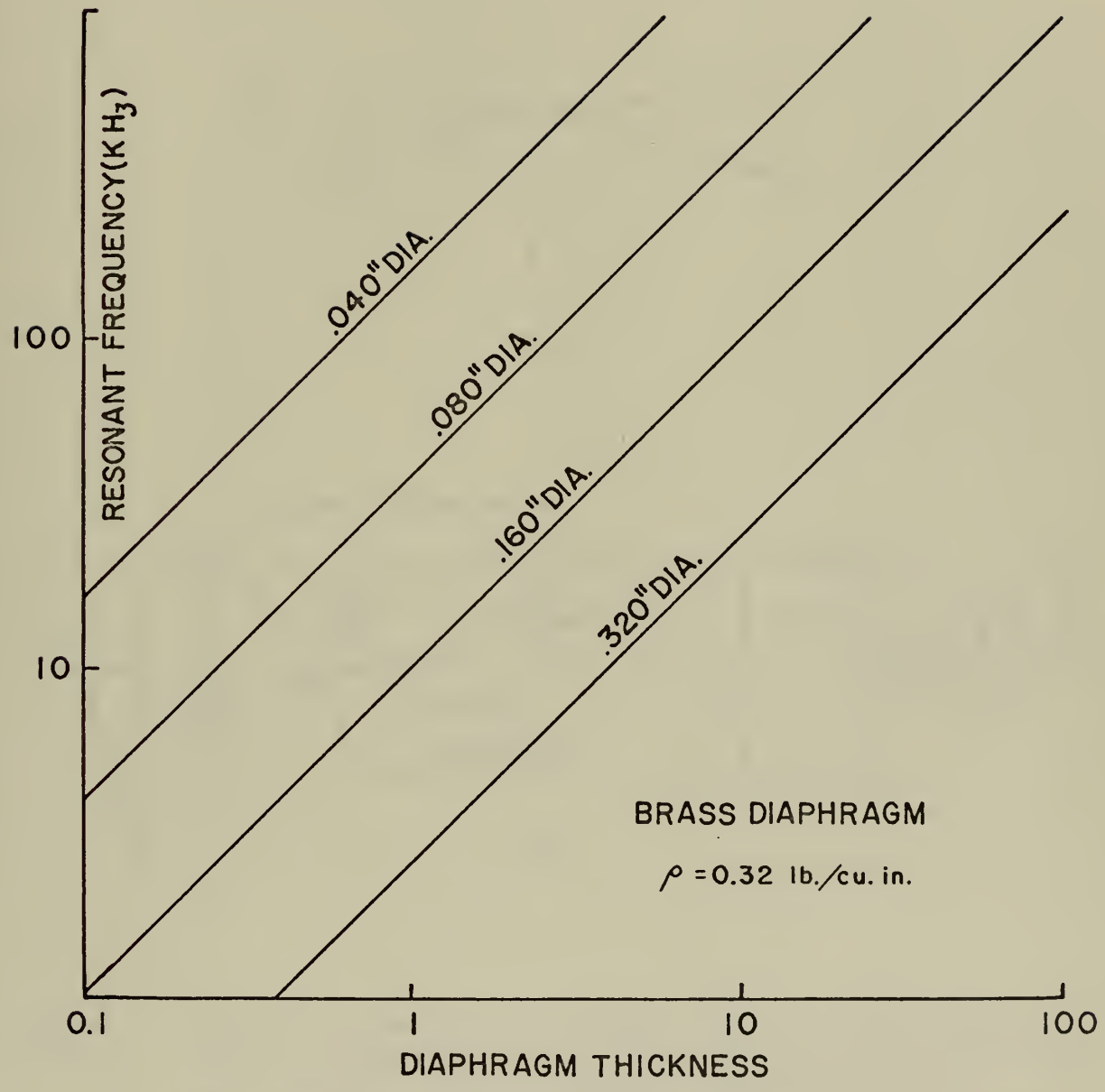

Figure 2c. Diaphragm Fundamental Resonant Frequency, Brass

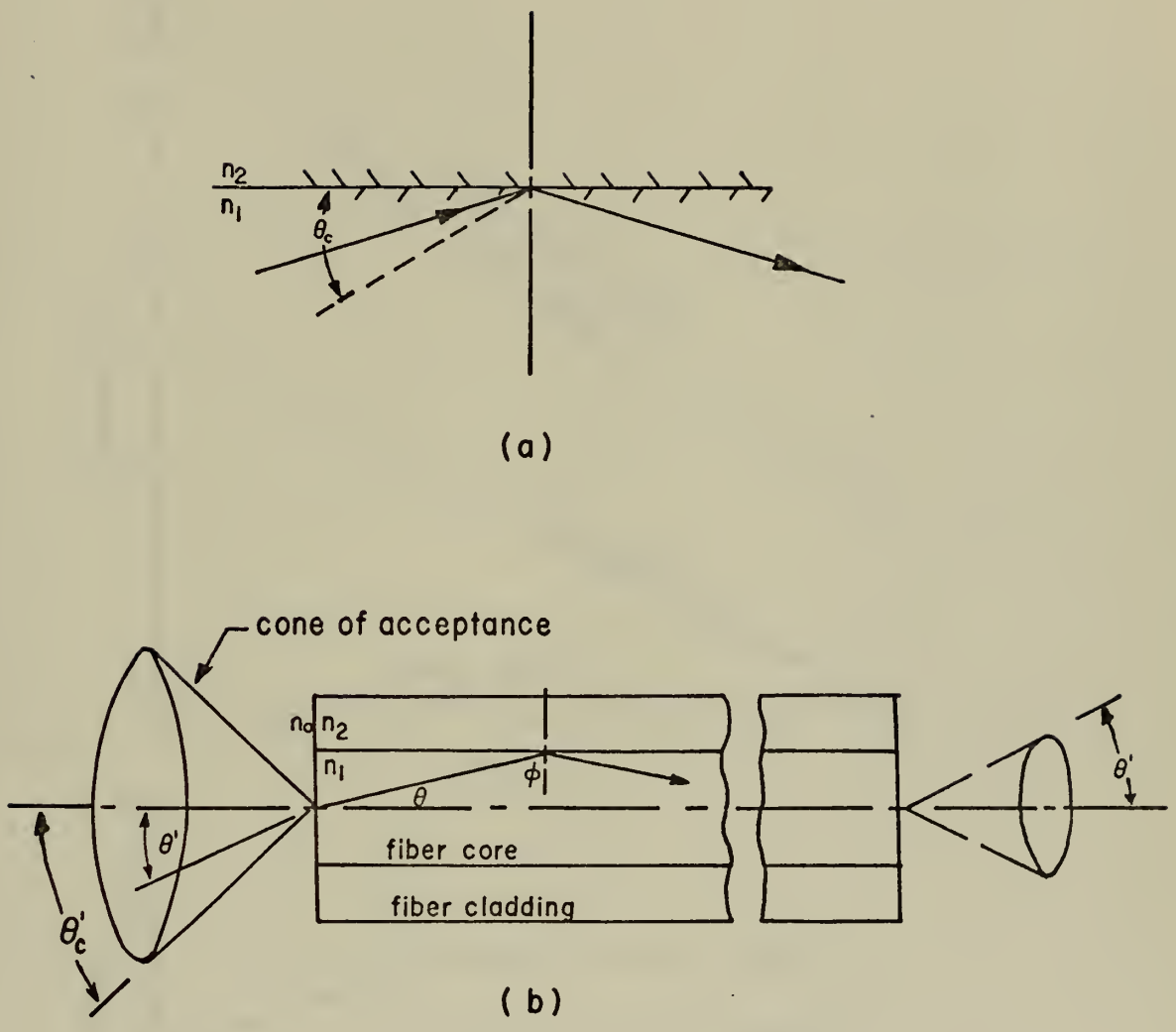

Figure 3. Light Transmission by Total Internal Reflection of Meridional Rays. (a) Total reflection corresponds to an angle $\theta_2=0$ or $\theta_c=\sin^{-1}[\sqrt{n_1^2-n_2^2}/n_1]$. (b) Total internal reflection in terms of incident angles corresponds to $\theta' \leq \theta_c' = \sin^{-1}[\sqrt{n_1^2-n_2^2}/n_0]$.

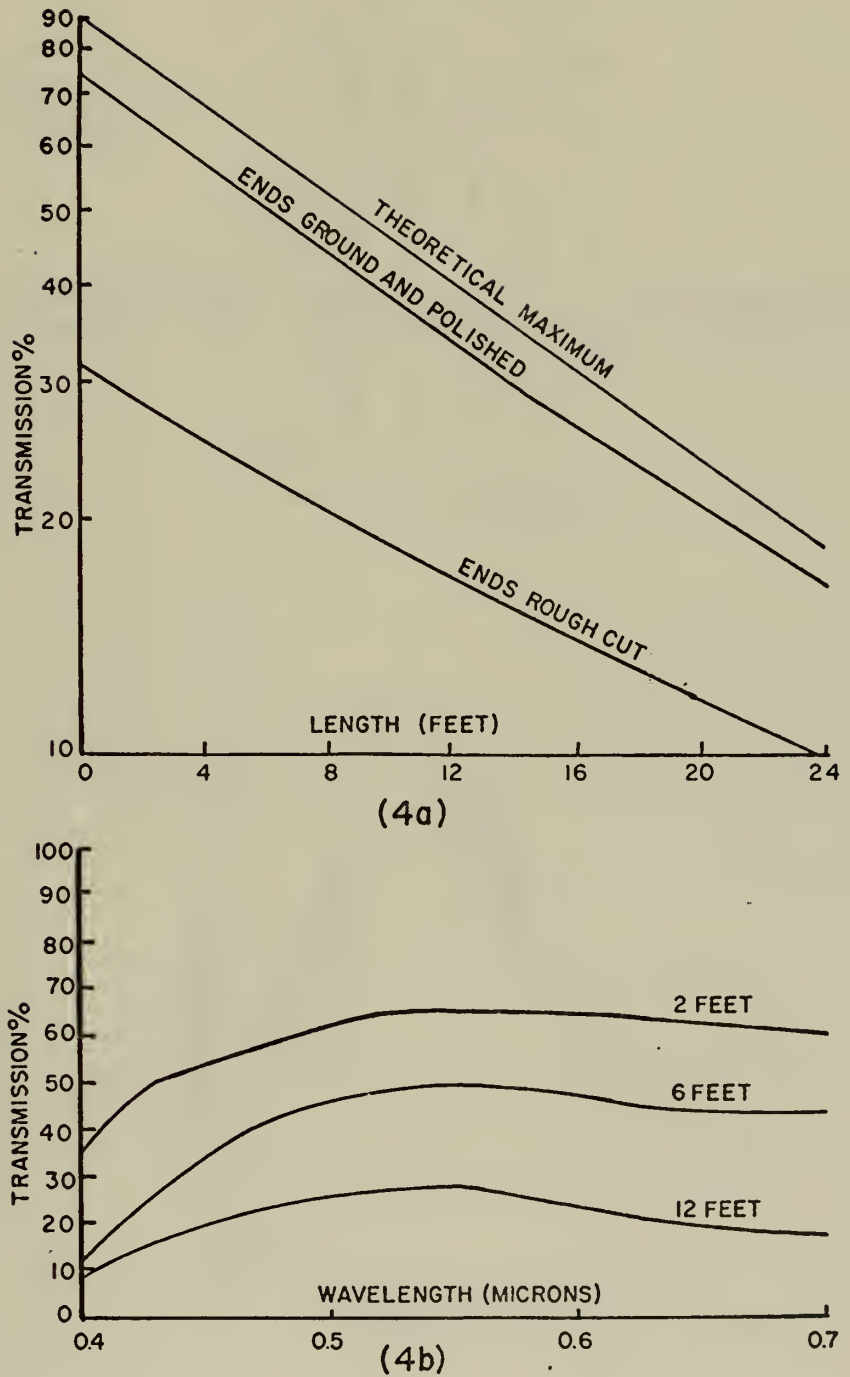

Figure 4. Transmission vs. Length and Wavelength for a Glass Fiber Bundle.

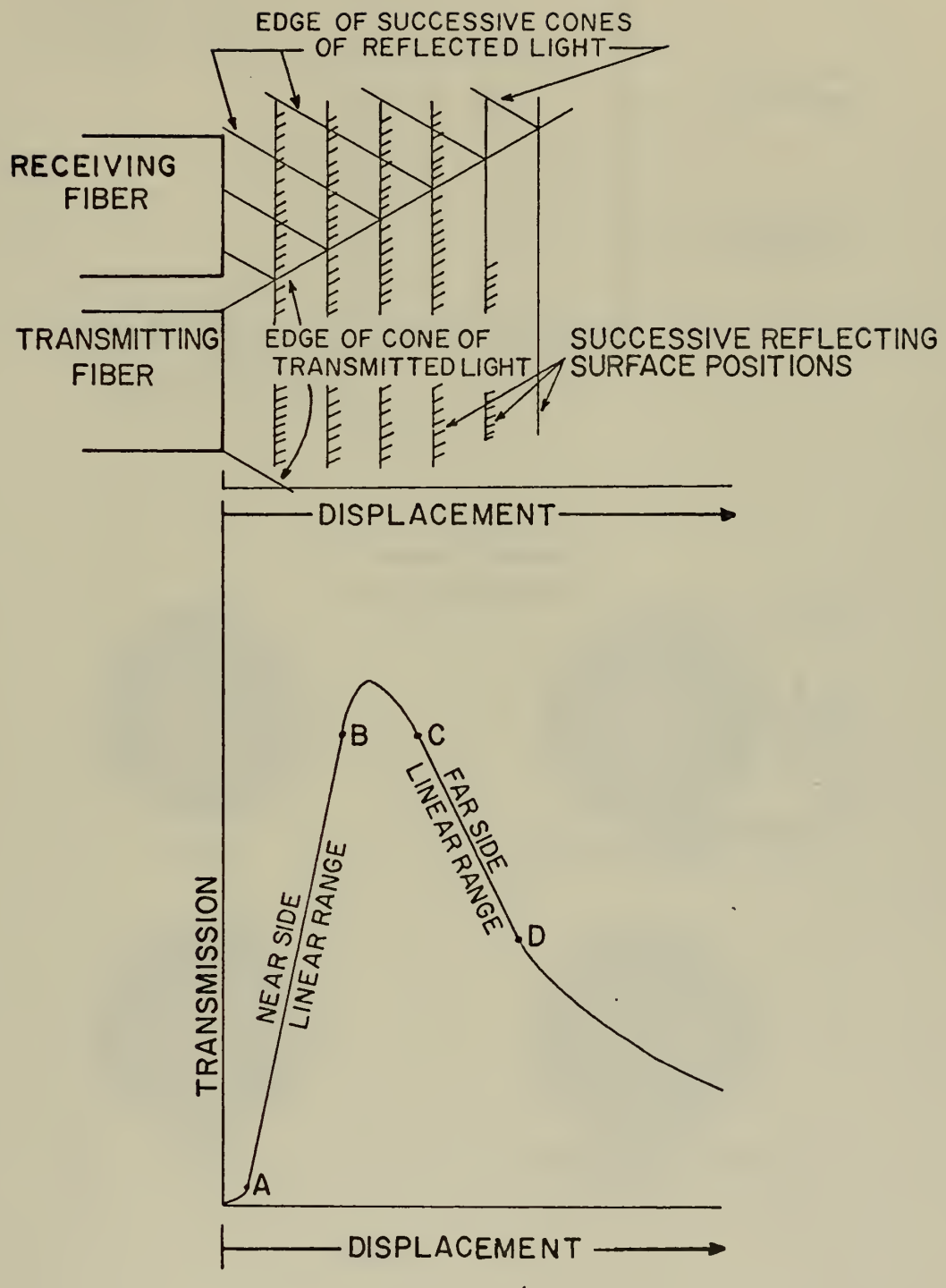

Figure 5. Principle of Displacement Measurement

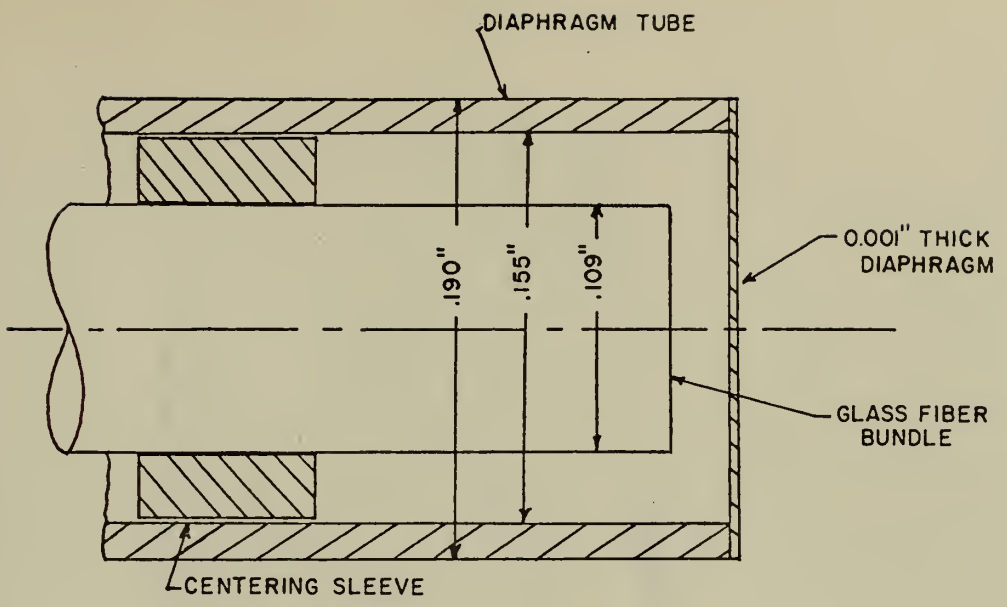

(6a)

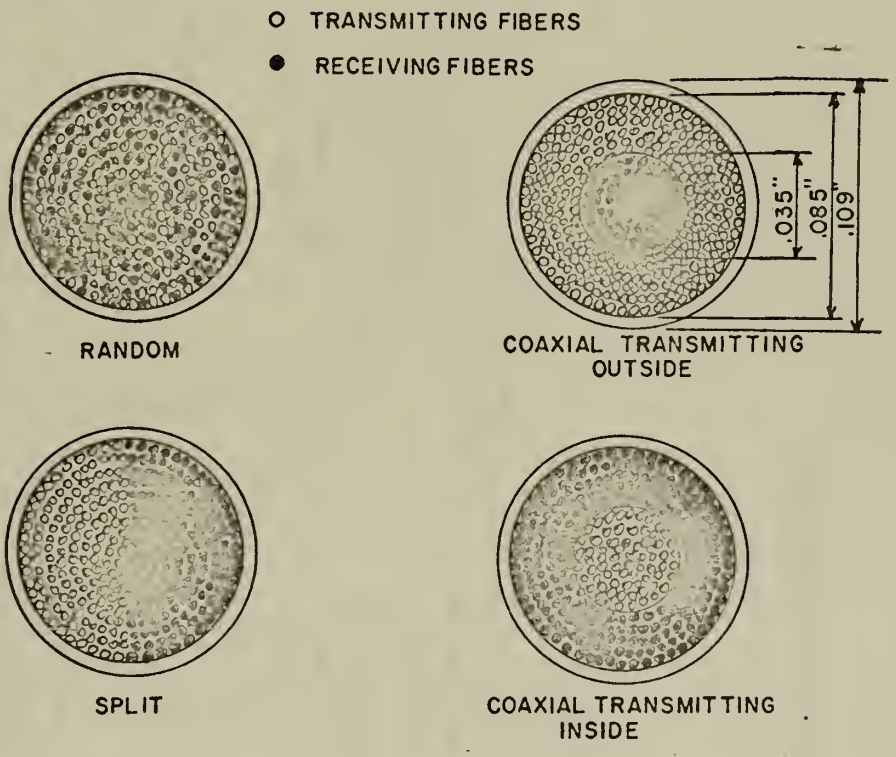

(6b)

Figure 6. Transducer Probe Design; a. Transducer Geometry, b. Various Fiber Distributions

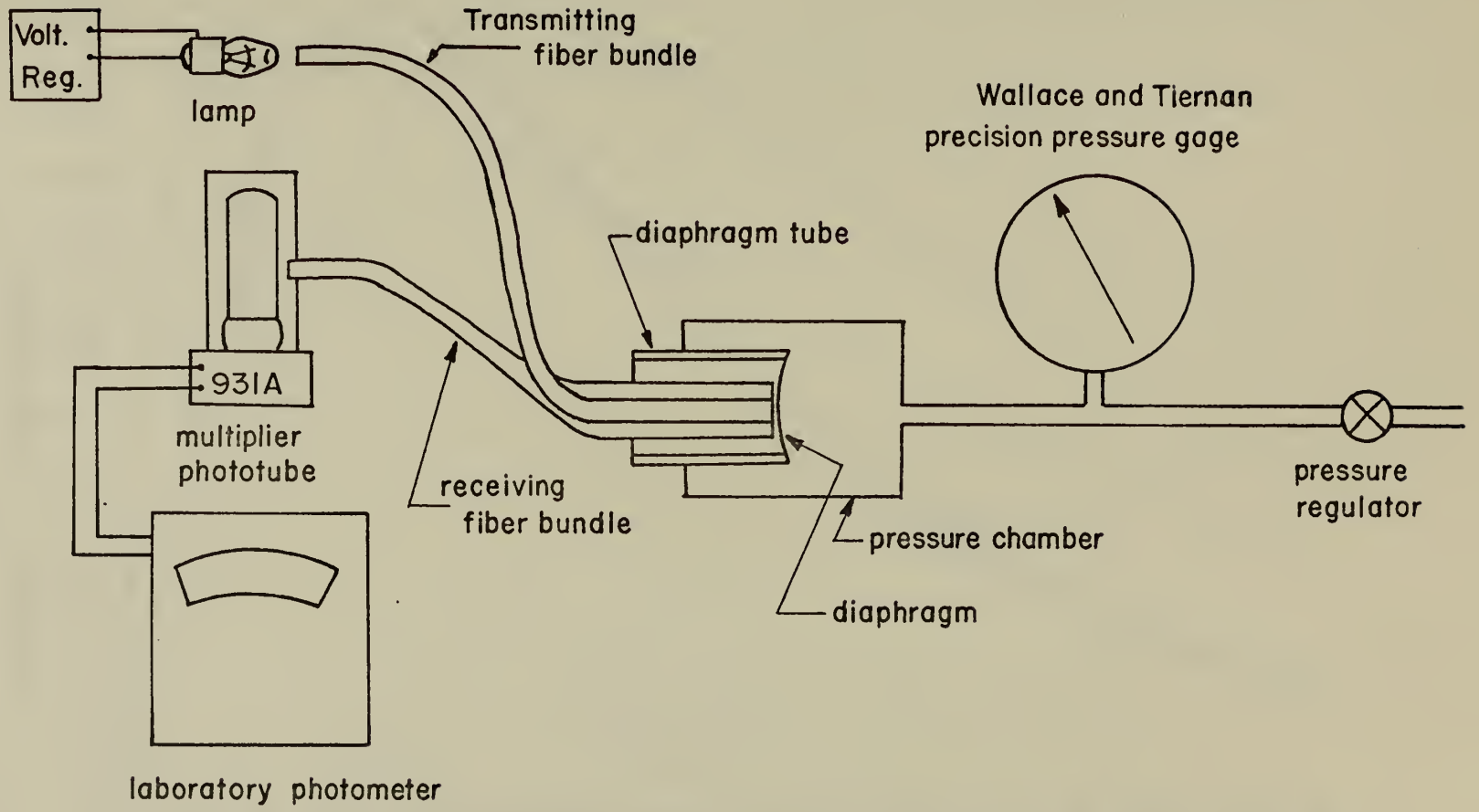

Figure 7. Experimental Arrangement (CTI Probe Illustrated)

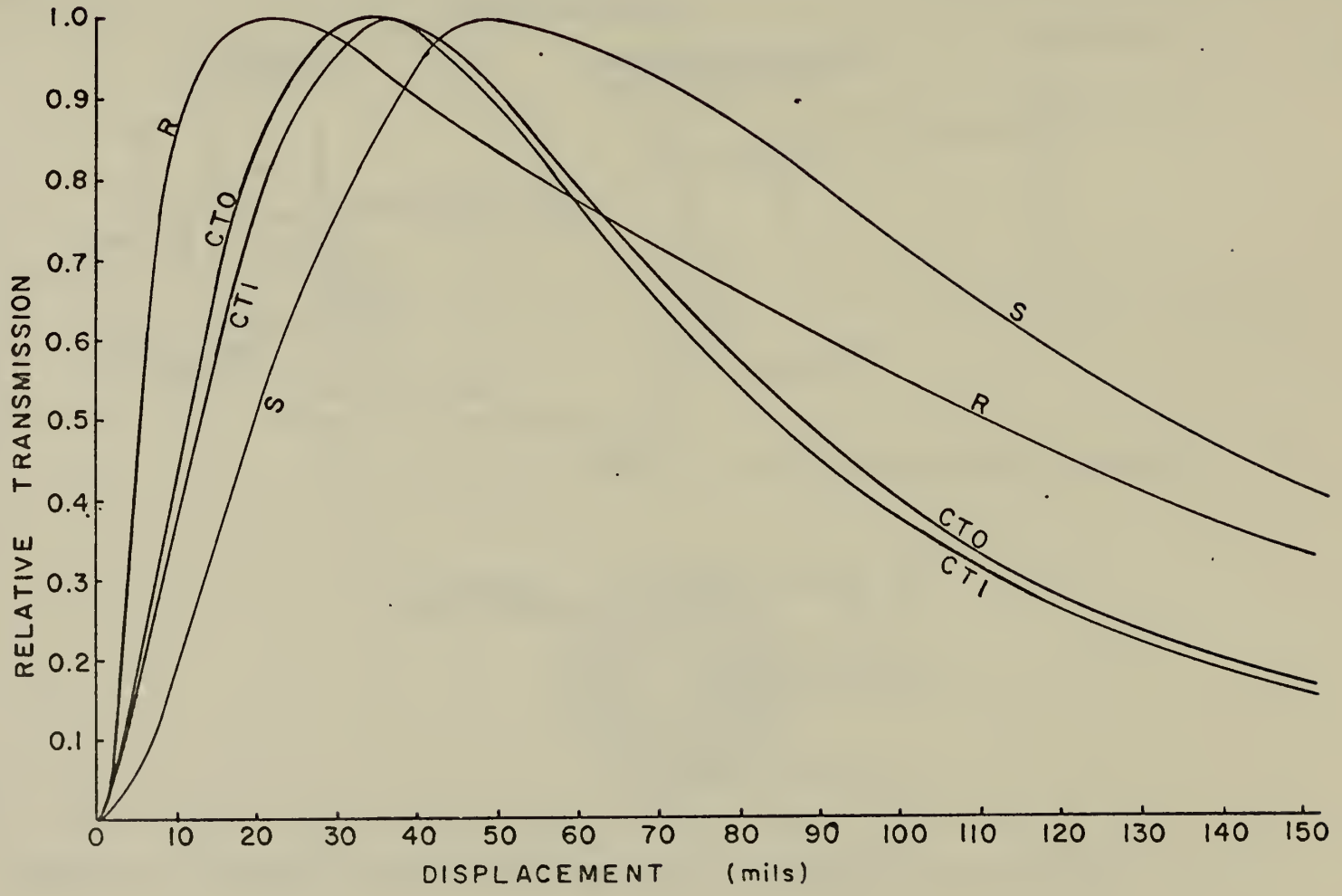

Figure 8. Linear Displacement Curves

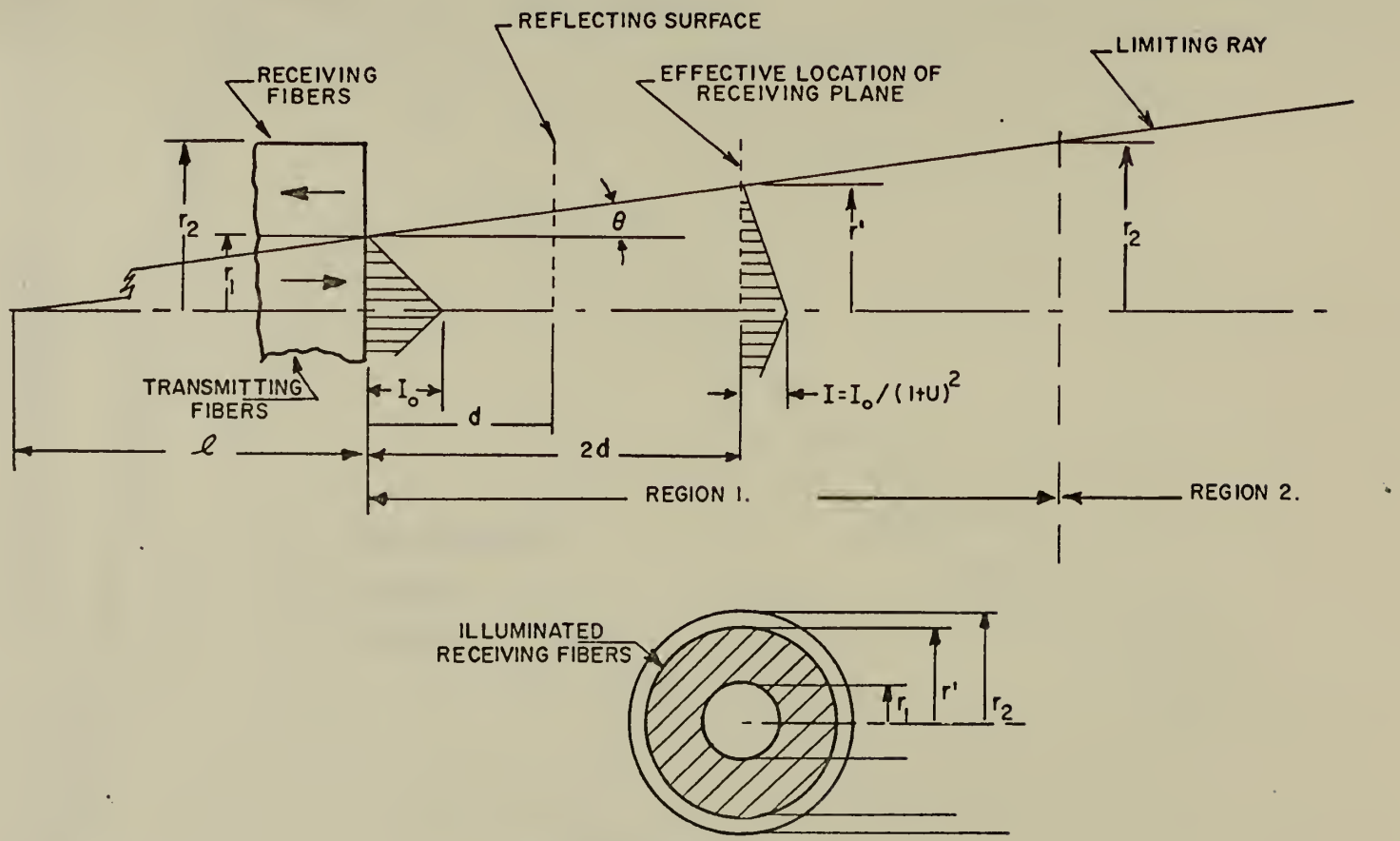

Figure 9. Geometry for Analysis of Optical Coupling for CTI Fiber Bundle

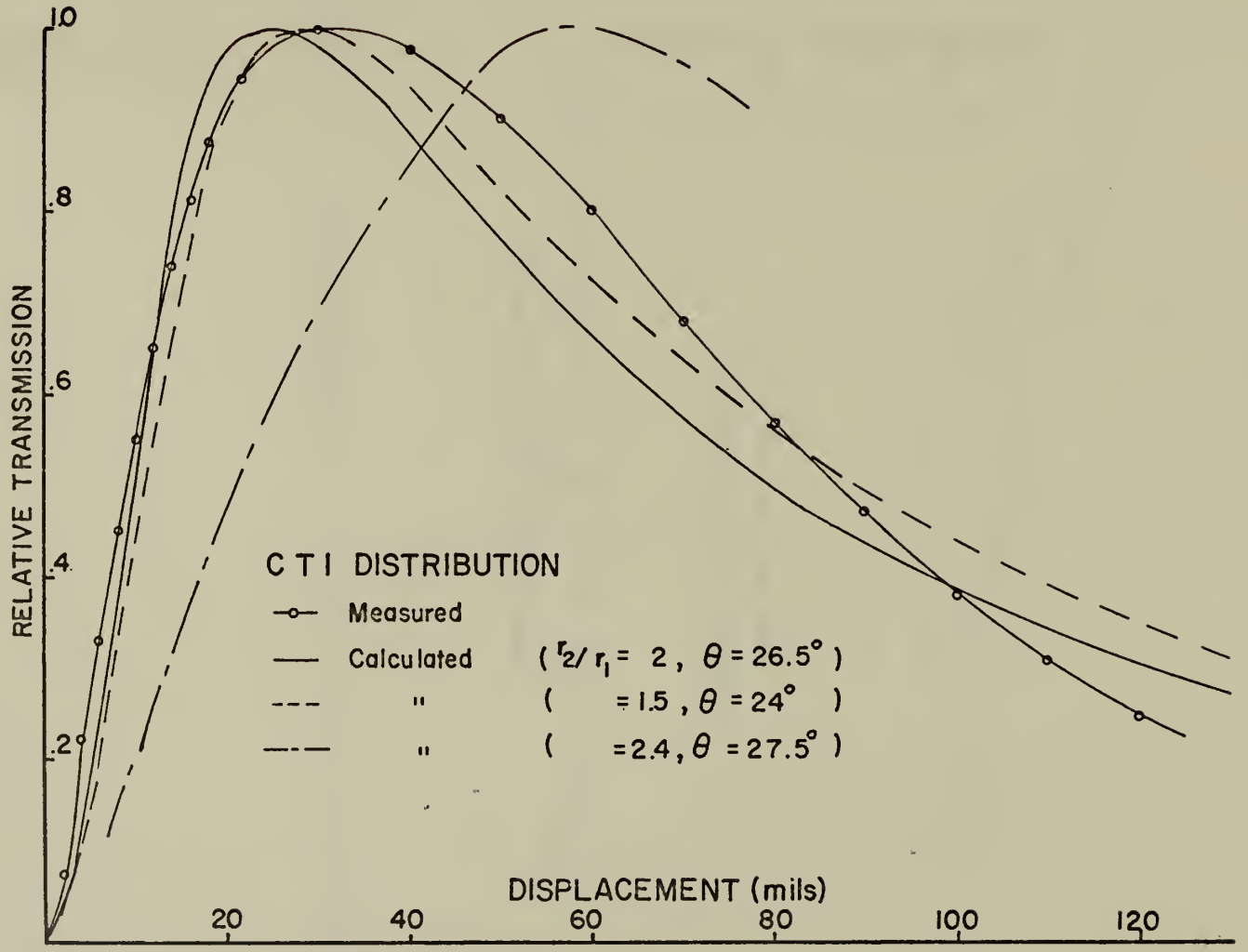

Figure 10. Calculated and Measured Displacement Curves

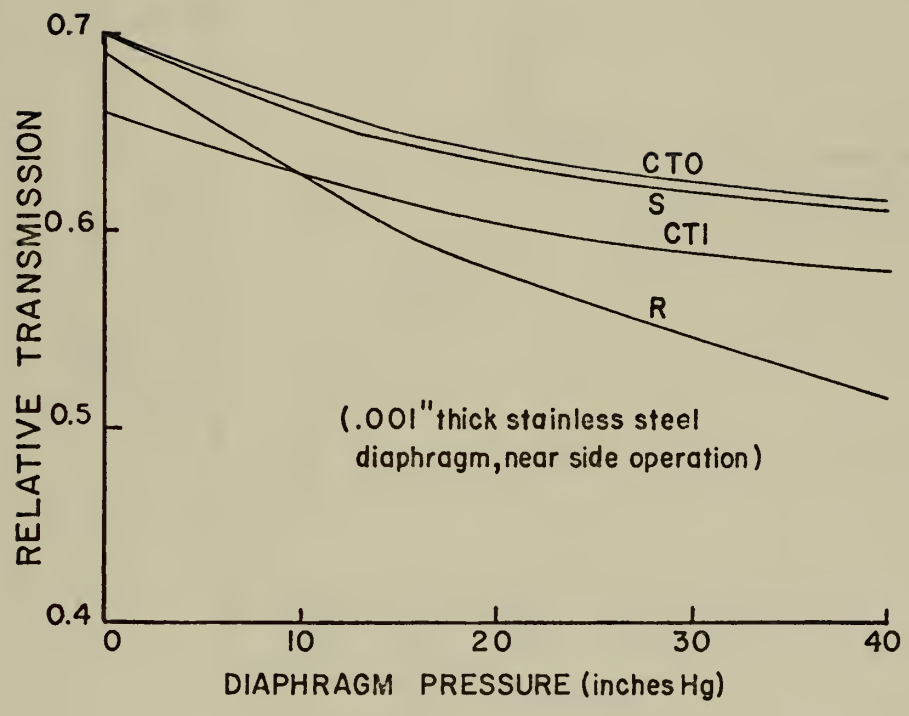

Figure 11. Transmission vs. Pressure Plots for Various Probe Geometries

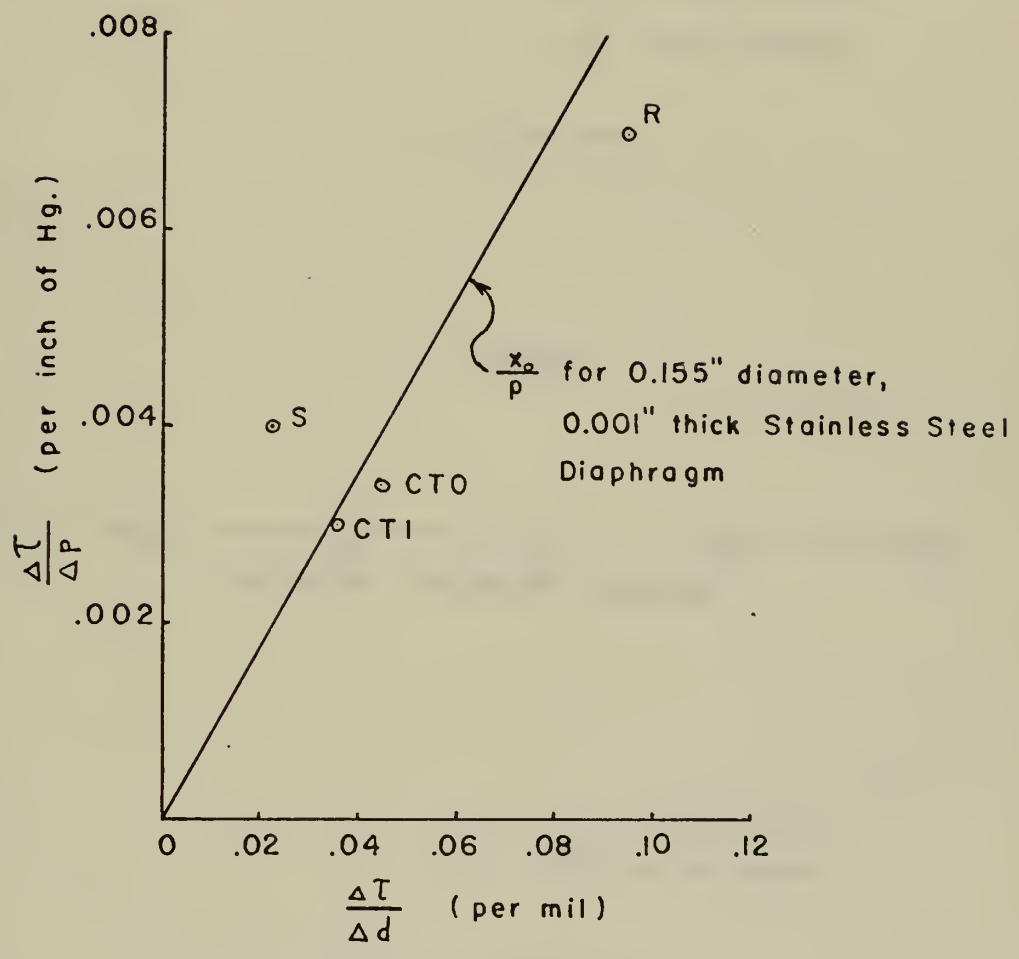

Figure 12. Rate of Change of Relative Transmission Per Inch of Mercury vs. Rate of Change of Relative Transmission Per Mil Displacement

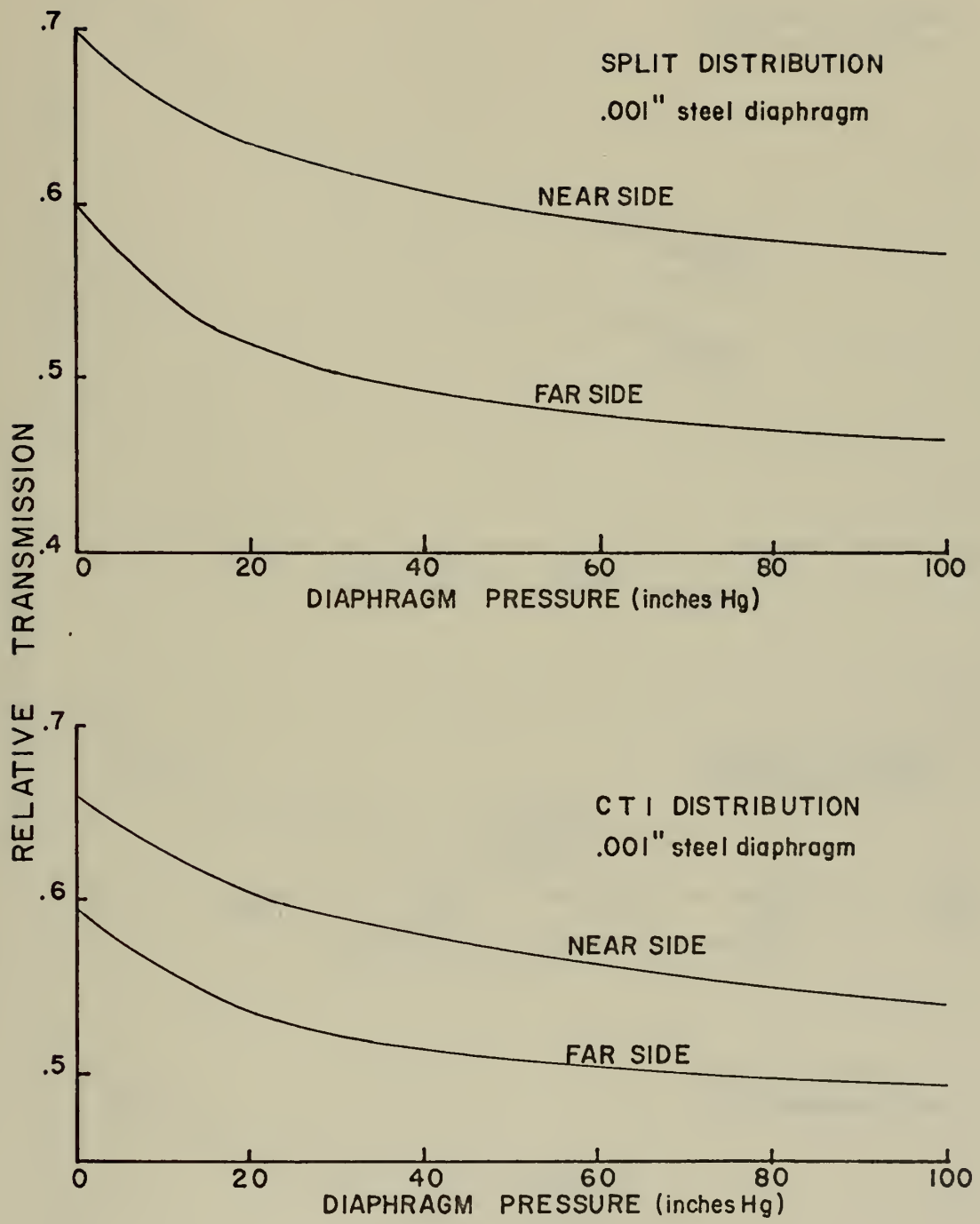

Figure 13. Transmission vs. Pressure Plot for Two Fiber Distributions for Near and Far Side Operation

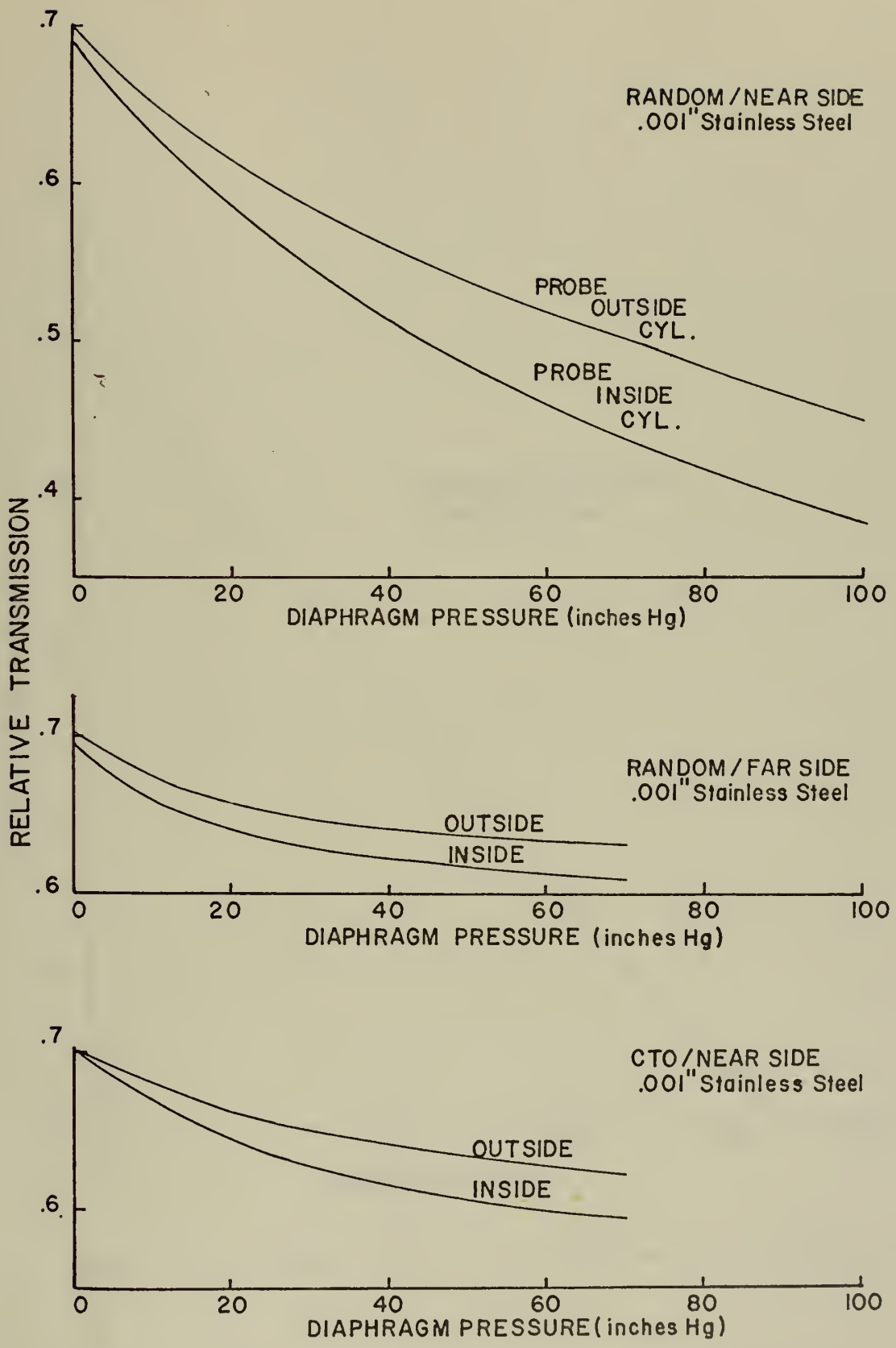

Figure 14. Wall Reflection Effects for Several Fiber Distributions

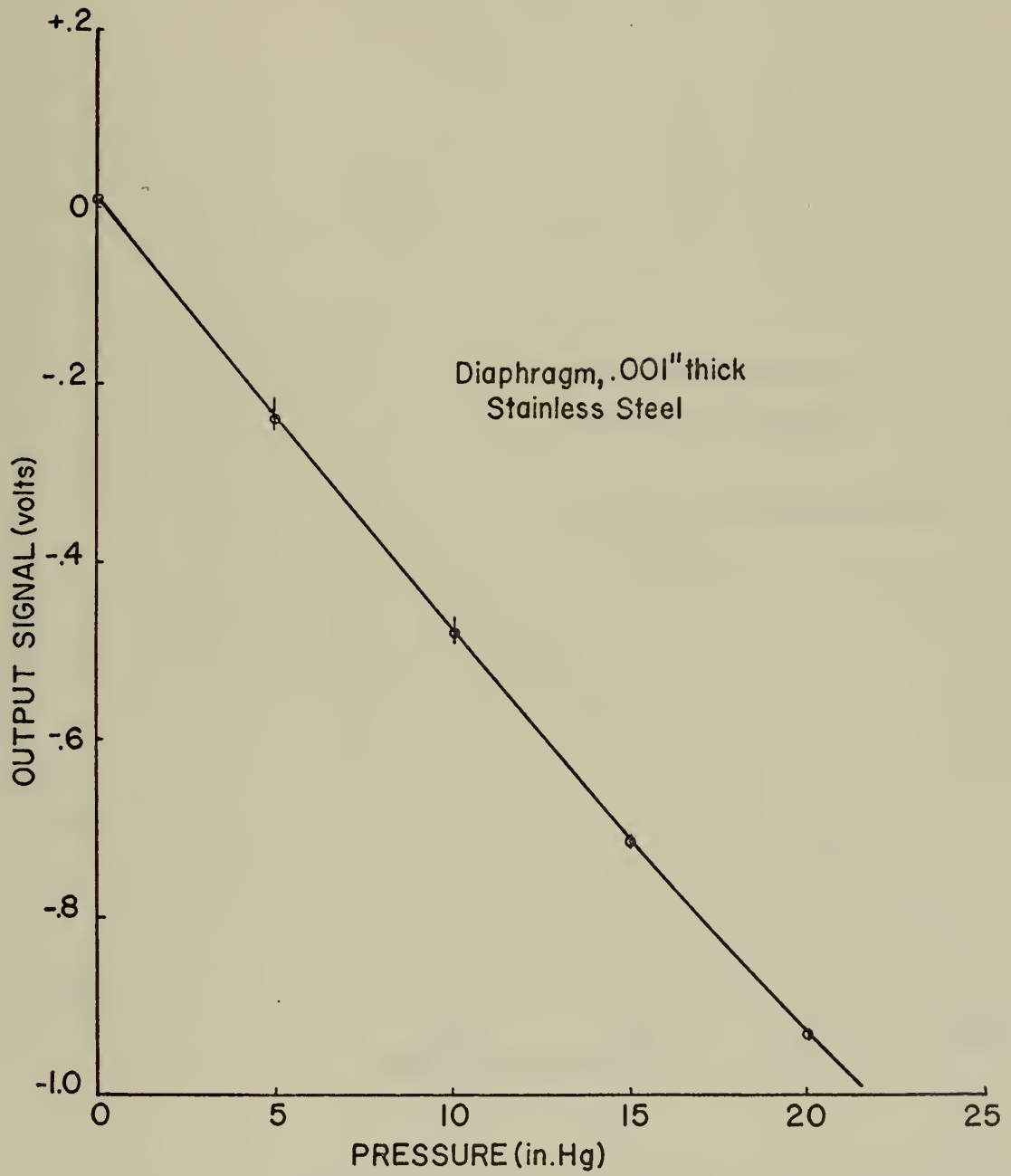

Figure 15. Output Signal vs. Pressure for a Random Probe

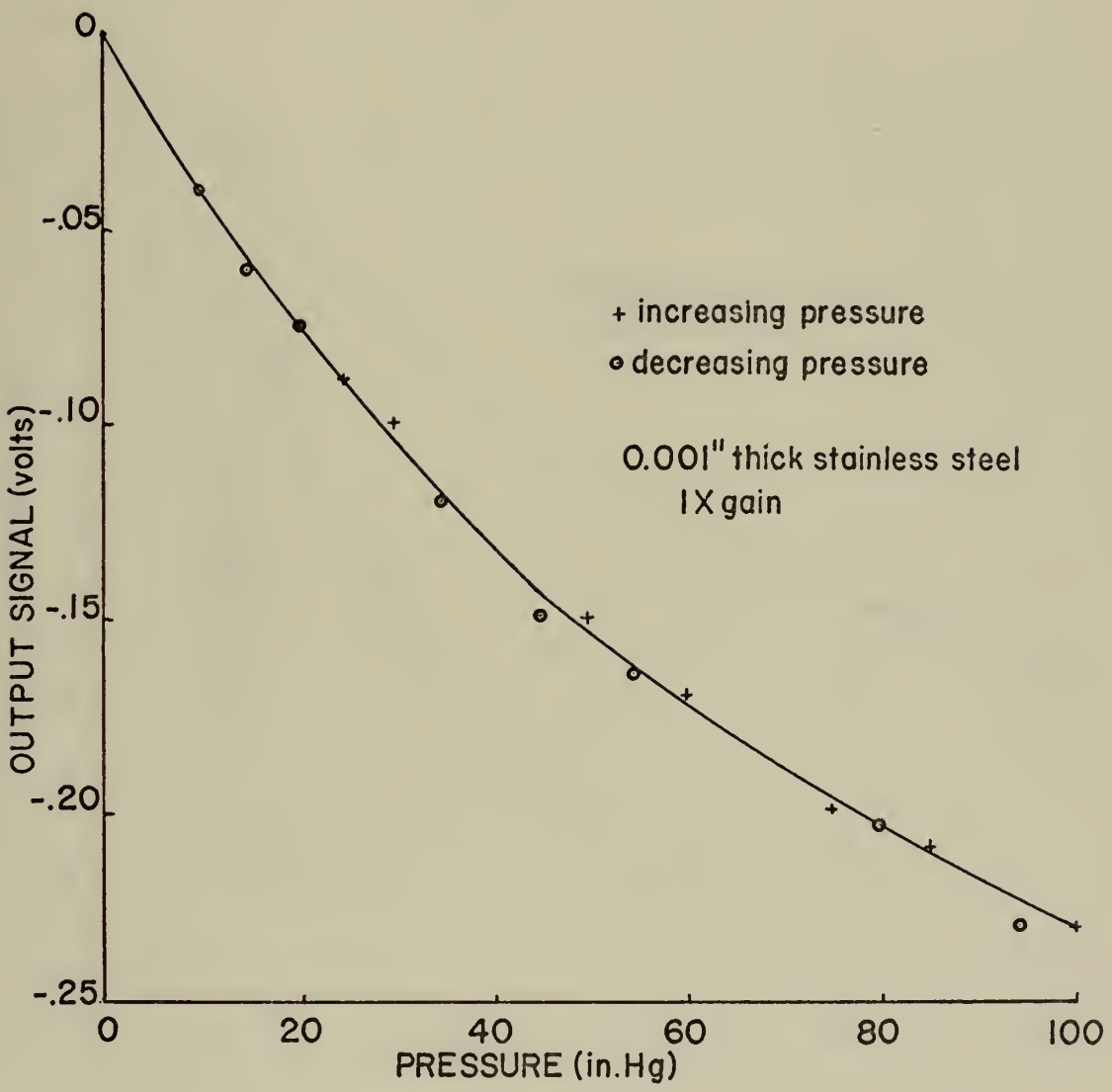

Figure 16. Output Signal vs. Pressure for a CTI Probe

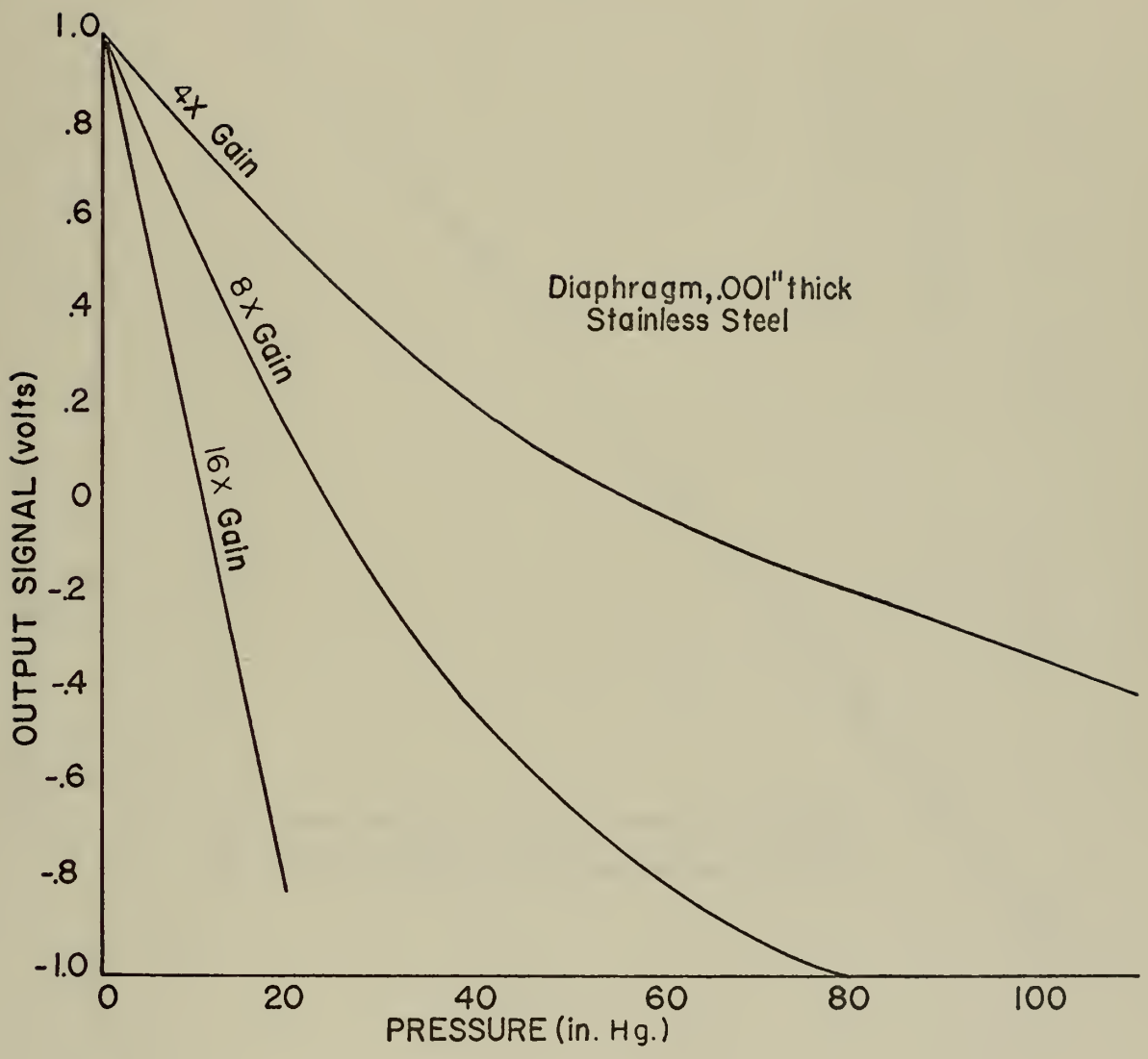

Figure 17. Output Signal vs. Pressure for a CTO Probe Using Various Instrument Gain Settings

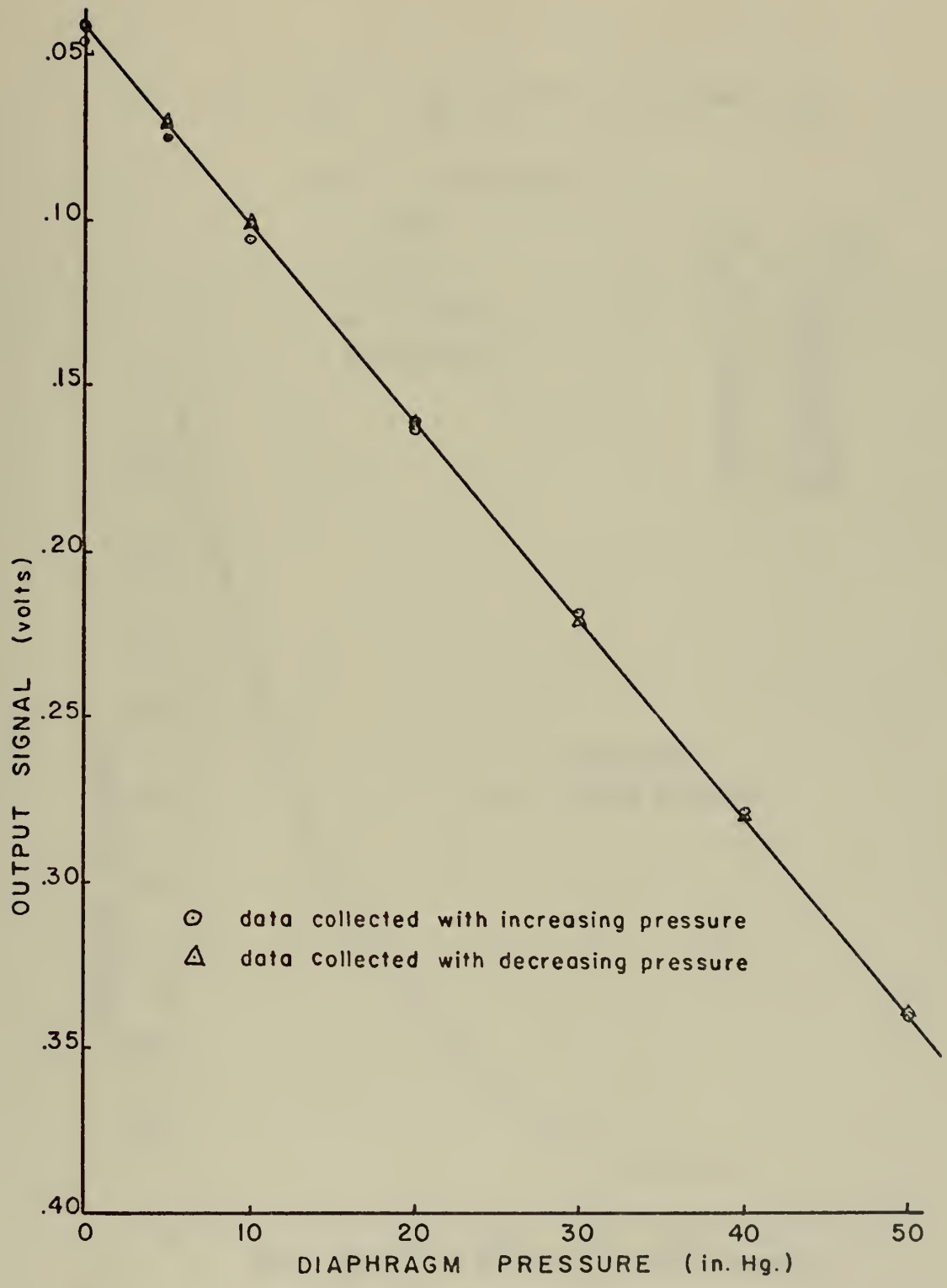

Figure 18. Output Signal vs. Pressure for a Random Probe (0.003") thick brass diaphragm, near side, 1X gain)

$$\ln\left(\frac{I}{I_0}\right) \sim \frac{L}{2a} \ln \alpha \tan\theta - \beta L \sec\theta + \beta L$$

$$\sin\theta = (1/n_1)\sin\theta'$$

$L = 36''$

$2a = 0.003$

$\alpha = 0.9993$

$\beta = 0.085/\text{ft.}$

θ'	$\ln\left(\frac{I}{I_0}\right)$
0	1.0
5	.636
10	.404
15	.256
20	.162
25	.102
30	.065
34	.045

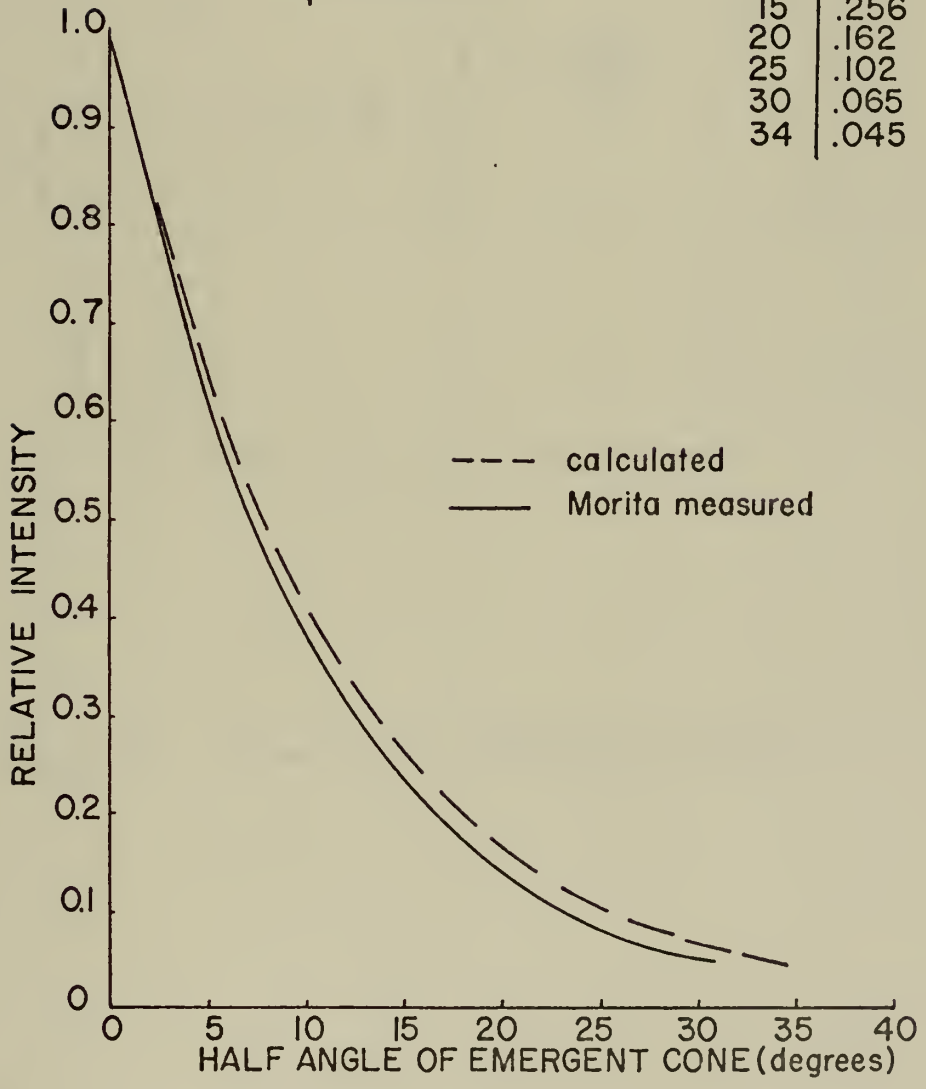

Figure 19. Angular Intensity Distribution of Emergent Light

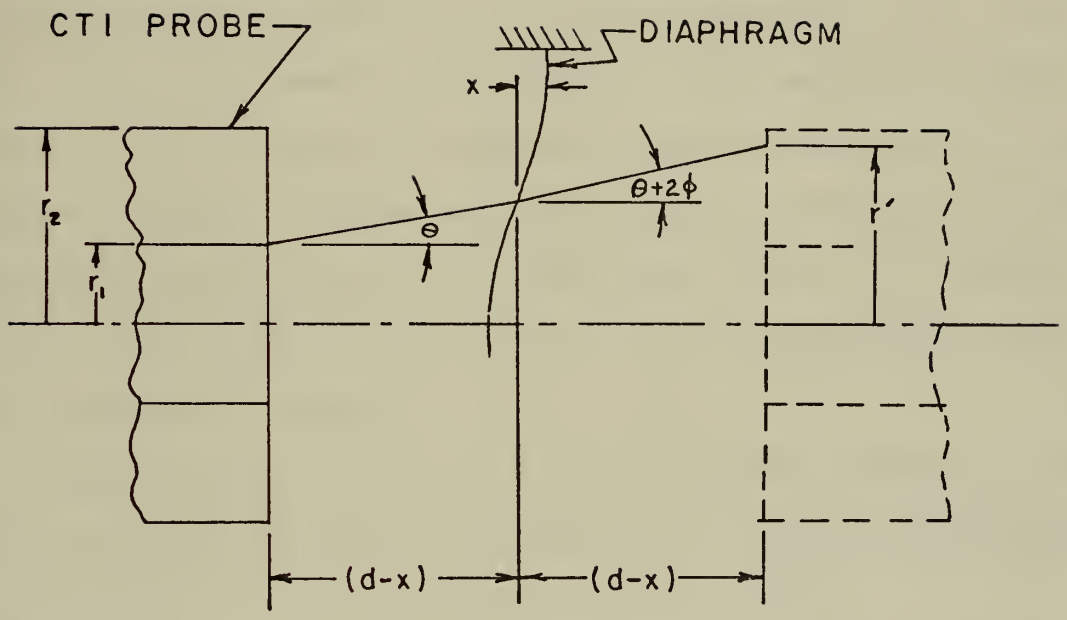

Figure 20. Geometry for Diaphragm Analysis

APPENDIX A

DISTRIBUTION OF LIGHT EMITTED FROM THE OPTIC FIBER

The ratio of transmitted intensity to the incident intensity of a light ray was given by equation (9). Using this equation the emitted intensity distribution relative to the maximum emitted intensity at $\theta=0$ was calculated for a single fiber of 3 mil diameter, 36" long and half angle acceptance cone of 34°. A constant incident intensity distribution was assumed. Typical values used for internal reflectivity and absorption coefficient were 0.9993 and 0.085 $ft.^{-1}$ respectively. The transmission factor, T, was considered a constant and, therefore, ignored.

Since equation (9) is in terms of angles internal to the fiber core and the result was desired in terms of exit angles, Snell's law was used to relate the two angles.

The results of these calculations are shown in Figure 19. Morita [15] calculated and measured an angular distribution for 0.6 mil fibers of the same NA arranged in a circular cross section, the result of which is also shown in Figure 19. The above calculations correspond reasonably well with Morita's measurements. Intensity attenuation at off axis angles is seen to be greater with smaller diameter fibers.

The actual emitted light from the CTI probe was a cone of half angle of approximately 27.5°.

APPENDIX B

LIMITING RAY ANALYSIS FOR CTI DISTRIBUTION

Consider an emitted light ray exiting the source fibers at a radius r_1 and angle θ as in Figure 20. After reflection from a flat surface at a distance, d, from the source, the ray intersects the receiving fiber entrance area at a radius, r, where

$$r = r_1 + 2d \tan \theta . \tag{10}$$

For a curved reflecting surface the radius of the corresponding intersecting point was given by the equation

$$r' = r_1 + (d-x)[\tan \theta + \tan (\theta+2\phi)] \tag{11}$$

where x and ϕ represent the deflection and slope respectively of the diaphragm at the point of ray reflection. The quantity (r'-r) represents the difference between the flat plate and a pressure diaphragm. Equation (11) was reduced to

$$r' = r_1 + 2(d-x)[\tan \theta + \phi(1 + \tan^2 \theta)] \tag{12}$$

by neglecting the ϕ^2 term and approximating $\tan(\theta+2\phi)$ by $(\tan \theta + 2\phi)(1 + 2 \tan \theta)$. Then (r'-r) becomes

$$r'-r = \Delta r = 2(1 - \frac{x}{d})d \ (1 + \tan^2 \theta) - 2x \tan \theta . \tag{13}$$

For the approximation $d \doteq 2x$ and $\tan \theta \doteq 0.5$,

$$\Delta r = -x(1 - 2.5\phi) . \tag{14}$$

Therefore when ϕ is less than 0.04, the diaphragm slope has a negligible effect compared to the diaphragm linear displacement for near side operation. For deflections less than half the plate thickness, the maximum diaphragm slope occurs at a radius equal to 0.58 times the diaphragm radius. The maximum slope was approximately $\phi_{max} = 2t/D$, which for 1 mil thickness and 0.155" diameter becomes $\phi = 0.013$ radians. The diaphragm slope was negligible for near side operation. A more accurate analysis, however, might consider area differences by the term $(r'^2 - r^2)$.

APPENDIX C

OUTPUT SIGNAL FOR TRANSLATION OF FLAT REFLECTING SURFACE

A CTI fiber bundle is considered to be emitting light as a point source from a location some distance, ℓ, measured internally from the exit plane of the bundle, Figure 9. The intensity at any position, 2d, is expressed in terms of the exit plane intensity as

$$I = I_0/(1 + 2d/\ell)^2 \qquad (15)$$

which may be written as

$$I = I_0/(1 + u)^2 \qquad (16)$$

where $u = (2d/r_1)\tan\theta$, since $\ell = r_1 \cot\theta$.

From the results of Appendix A a triangular intensity distribution for $0 \leq r \leq r_1$ as shown was considered to be a suitable approximation. A triangular distribution was chosen for ease of integration. The total light flux entrapped by the receiving fibers was expressed as

$$F = \int_{r_1}^{r'} I(r)\, 2\pi r\, dr \qquad (17)$$

where $I(r) = I[1 - (r/r_1) / (1 + u)]$. (18)

There are two distinct regions of interest defined by r' being either less than or greater than r_2. For the first region

($r' < r_2$) integration of equation (17) yields

$$F_1 = \frac{\pi I_0 r_1^2}{3} \left\{ \frac{u^2(3 + u)}{(1 + u)^3} \right\} \qquad (19)$$

for $u \leq R-1$ and $R = r_2/r_1$. In the second region ($r' > r_2$) the upper limit on the integral becomes constant and equal to r_2. Integration then gives the result

$$F_2 = \frac{\pi I_0 r_1^2}{3} \left\{ \frac{3u(R^2-1) - (2R^3-3R^2+1)}{(1 + u)^3} \right\} \qquad (20)$$

for $u \geq R-1$.

Using several values of R and θ, a plot of these equations normalized to 1.0 at the maximum value is given in Figure 10.

LIST OF REFERENCES

1. Hazell, C. R. and Engel, S. L., "A Fiber Optical Angular Displacement Transducer," Journal of Scientific Instruments, v. 2, series 2, p. 110-111, 1969.

2. Defense Atomic Support Agency Report 2036, Vol-1, A Fiber Optic Pressure Transducer for Use in Ionizing Radiation Environments, by B. I. Davis, Northrop Corporate Laboratories, January, 1968.

3. Maine, R. E. and Lewis, D. W., "Pressure Transducer for Prosthetics," IEEE Transactions on Industrial Electronics and Control Instrumentation, v. 17, n. 2, p. 138, April, 1970.

4. Menadier, C., Kissinger, C. and Adkins, H., "The Fotonic Sensor," Mechanical Technology, Inc. Bulletin #02-100.

5. Morse, P. M., Vibration and Sound, p. 173-178, McGraw-Hill, 1948.

6. Mechanical Technology Inc., Specifications Sheet, "KD-100 Fotonic Sensor." Personal correspondence.

7. Siegmund, W. P., and others, Applied Optics and Optical Engineering, v. 4, pt. 1, p. 1-13.

8. Potter, R. J., "Transmission Properties of Optical Fibers," J. Opt. Soc. Am., v. 51, n. 10, p. 1079-1089, October, 1961.

9. Sattarov, D. K., "Propagation of Radiation Through Fiber-Optical Bundles," Sov. J. Opt. Tech., v. 5, p. 371, 1967.

10. Sattarov, D. K., "Numerical Apertures of Transparent Fiber Bundles," Sov. J. Opt. Tech., v. 4, p. 763, 1967.

11. Moross, G. G., "Applications of Non-Imaging Flexible Fiber Optics in Medicine and Dentistry," S.P.I.E. Seminar Proceedings, Fiber Optics, v. 14, Baltimore, Md., 1958.

12. Hsu, T. R., Moyer, R. G. and Banks, F. B., "A High Temperature Fibre-Optical Displacement Probe," Journal of Scientific Instruments, v. 2, Series 2, p. 1132, 1969.

13. Hsu, T. R. and Moyer, R. G., "Application of Fiber Optics to Holography," Applied Optics, v. 10, p. 669, March, 1971.

14. Den Hartog, J. P., Advanced Strength of Materials, p. 136-140, McGraw-Hill, 1952.

15. Morita, E., and Takase, M., "Angular Distribution of Light Emitted from the Optical Fiber Bundle," Japan J. Appl. Phys., v. 6, p. 414-415, 1967.

INITIAL DISTRIBUTION LIST

		No. Copies
1.	Defense Documentation Center Cameron Station Alexandria, Virginia 22314	2
2.	Library (Code 0212) Naval Postgraduate School Monterey, California 93940	2
3.	Chairman, Department of Aeronautics (Code 57) Naval Postgraduate School Monterey, California 93940	1
4.	Professor A. E. Fuhs, Code 57Fu Department of Aeronautics Naval Postgraduate School Monterey, California 93940	5
5.	Professor R. P. Shreeve, Code 57Sf Department of Aeronautics Naval Postgraduate School Monterey, California 93940	1
6.	LCDR Gordon W. Margerum Code 31 Naval Postgraduate School Monterey, California 93940	1
7.	Mr. Karl Guttmann Code 330 Naval Air Systems Command Washington, D. C. 20360	1
8.	Mr. Irv Silver Code 03 Naval Air Systems Command Washington, D. C. 20360	1
9.	Dr. Frank Tanczos Code 03 Naval Air Systems Command Washington, D. C. 20360	1
10.	Mr. Eric Lister Research and Technology Naval Air Propulsion Test Center Trenton, New Jersey 08628	1

11. Mr. Albert Martino — 1
Research and Technology
Naval Air Propulsion Test Center
Trenton, New Jersey 08628

12. Mr. Albert G. Powers — 1
NASA Lewis Research Center
Cleveland, Ohio 44135

13. Mr. Joseph Batka — 1
AFAPL/TBC
Wright-Patterson AFB, Ohio 45433

14. Mr. Harry Snowball — 1
AFFDL
Wright-Patterson AFB, Ohio 45433

15. Dr. Hans Von Ohain — 1
Chief Scientist
ARL
Wright-Patterson AFB, Ohio 45433

16. Mr. Terry Trumble — 1
AFAPL
Wright-Patterson AFB, Ohio 45433

17. Mr. Robert A. Langworthy — 1
Eustis Directorate
SAVDL-EV-PP
USAAMRDL
Fort Eustis, Virginia 23604

18. LCDR R. D. Matulka — 1
Office of Naval Research
Code 430C
Arlington, Virginia 22217

Security Classification

DOCUMENT CONTROL DATA - R & D

(Security classification of title, body of abstract and indexing annotation must be entered when the overall report is classified)

1. ORIGINATING ACTIVITY (Corporate author)	2a. REPORT SECURITY CLASSIFICATION
Naval Postgraduate School Monterey, California 93940	Unclassified
	2b. GROUP

3. REPORT TITLE

A Fiber Optic Pressure Transducer

4. DESCRIPTIVE NOTES (Type of report and inclusive dates)

Aeronautical Engineer's Thesis; June 1972

5. AUTHOR(S) (First name, middle initial, last name)

Gordon William Margerum

6. REPORT DATE	7a. TOTAL NO. OF PAGES	7b. NO. OF REFS
June 1972	63	15

8a. CONTRACT OR GRANT NO.	9a. ORIGINATOR'S REPORT NUMBER(S)
b. PROJECT NO.	
c.	9b. OTHER REPORT NO(S) (Any other numbers that may be assigned this report)
d.	

10. DISTRIBUTION STATEMENT

Approved for public release; distribution unlimited.

11. SUPPLEMENTARY NOTES	12. SPONSORING MILITARY ACTIVITY
	Naval Postgraduate School Monterey, California 93940

13. ABSTRACT

A pressure transducer with an outside diameter of 0.190" has been built and statically tested. The transducer used a glass fiber bundle 0.109" in diameter to transmit and receive reflected light from a pressure diaphragm. The amount of light returned to a photosensor was dependent upon the diaphragm shape and relative position from the optic fiber bundle. The response was linear over a pressure range which was dependent upon the diaphragm thickness. Several fiber optic probes with different fiber distributions were tested. The random fiber distribution gave the greatest sensitivity. However, with suitable choice of gain selection, pressure range could be sacrificed for increased pressure resolution for any combination of fiber distribution and diaphragm thickness.

A theory was developed for a coaxial fiber distribution with the source light transmitted by the inner circle of fibers and operating with reflection from a flat surface. The theory provided a response curve shape which compared with the measured response.

DD FORM 1 NOV 65 1473 (PAGE 1)

S/N 0101-807-6811

Security Classification

A-31408

14. KEY WORDS	LINK A		LINK B		LINK C	
	ROLE	WT	ROLE	WT	ROLE	WT
fiber optics						
pressure transducer						

DD FORM 1 NOV 65 1473 (BACK)

S/N 0101-807-6821